Alexandria Engineering Journal 129 (2025) 515–529

Contents lists available at ScienceDirect

Alexandria Engineering Journal

journal homepage: www.elsevier.com/locate/aej

Original article

Heat and mass transfer analysis of a Bingham ternary nanofluid exposed to radiation over stretching/shrinking sheets and Stefan blowing effect

S.M. Sachhin [a], F.-J. Granados-Ortiz [b,*], U.S. Mahabaleshwar [a], J. Ortega-Casanova [c], L.M. Pérez [d]

[a] Department of Studies in Mathematics, Davangere University, Shivagangothri, Davangere 577 007, India
[b] Department of Engineering, University of Almeria, Cañada de San Urbano s/n, 04120 Almeria, Spain
[c] Department of Mechanical, Thermal and Fluid Engineering, University of Malaga, C/ Dr Ortiz Ramos s/n, 29071 Malaga, Spain
[d] Departamento de Ingeniería Industrial y de Sistemas, Universidad de Tarapacá, Casilla 7D, Arica 1000000, Chile

ARTICLE INFO

Keywords:
Stefan blowing
Porous media
Schmidt number
Thermal radiation
Ternary nanofluid

ABSTRACT

Advancements in engineering fields regarding the Stefan blowing effects on Bingham fluids have captured significant attention from both scientists and industry. However, there is scarce literature on Bingham ternary nanofluids under radiation and porous media with mixed boundary conditions. This study examines the Stefan blowing effect and Schmidt number on bi-viscous Bingham ternary nanofluid. The main novelty in this work is the analytical study of the impact of radiation over such nanofluid flow (*Cu*, *Ag*, and TiO_2 nanoparticles in sodium alginate) joint with the blowing effect, Schmidt numbers, and stretching/shrinking conditions. Results show that to increase the thermal radiation and Eckert number increased the temperature of the fluid flow, and when adding the ternary nanoparticles such effect was found to be strongly boosted. As the Eckert number increases, convection becomes more relevant, leading to an increase in temperature. Moreover, enhancing the volume fraction raises the temperature, enhancing the Schmidt number, which has strong relation to the temperature distribution of the nanofluid, Stefan blowing and concentration. Also, the Stefan blowing parameter was found to provide superior control over concentration in this ternary nanofluid, since the higher the blowing parameter, the more sensitive concentration is to the addition of the ternary nanoparticles.

1. Introduction

In the present study authors explored the effectiveness of ternary nanofluids containing titanium dioxide (TiO_2), copper (*Cu*) and silver (*Ag*) tiny particles. These specific nanoparticles were chosen for their remarkable properties that enhance both the heat and flow behaviors of the nanofluid. Copper and silver are renowned for their exceptional thermal conductivity, which significantly improves heat transfer, while TiO_2 provides a stable dispersion, further enhancing the nanofluid's performance under diverse conditions. When compared to other nanoparticles, this unique combination delivers a well-rounded improvement in both heat transfer efficiency and flow behavior, making it particularly effective in complex heat exchange systems. These nanoparticles are crucial for real-world applications such as cooling systems in electronics, energy-efficient industrial processes, and advanced thermal management in renewable energy technologies. Their ability to enhance heat transfer while maintaining stability under extreme thermal stresses makes them indispensable for optimizing system performance and efficiency across various industries. There is a vast literature on studies related to special performance of nanofluids. For instance, Sachhin et al. [1] explored the slip effect in a boundary layer nanofluid movement on porous sheet and found out that the slip effect reduces the momentum of the flow. Turkyilmazoglu [2] studied the Buongiorno model (aggregation of factors such as inertia, magnetic effect, fluid drainage, and gravity in nanofluid modelling) with the suspension of nanoparticles over the asymmetric channel and found that the combined effects of thermophoresis and Brownian motion had strong impact on the Nusselt number. Gkounta et al. [3] explored the influence of nanoparticles on an interface with radiation on a printed circuit and showed that radiation had an important role in the enhancement of temperature. Siddheshwar et al. [4] discovered the Rayleigh–Bénard convection with nanofluid on minimal mode Lorenz models and determined that the Lorentz force reduces the momentum of the flow, and Granados-Ortiz et al. [5]

* Corresponding author.
E-mail addresses: sachinsm030@gmail.com (S.M. Sachhin), fjgranados@ual.es (F.-J. Granados-Ortiz), u.s.m@davangereuniversity.ac.in (U.S. Mahabaleshwar), jortega@uma.es (J. Ortega-Casanova), lperez@academicos.uta.cl (L.M. Pérez).

https://doi.org/10.1016/j.aej.2025.06.026
Received 24 January 2025; Received in revised form 9 May 2025; Accepted 14 June 2025

Nomenclature

List of symbols	Descriptions[SI unit]
a	Stretching coefficient$[s^{-1}]$
A_1, A_2, A_3, A_4	Constants[-]
Ag	Silver[-]
C	Concentration$[\mathrm{mol}/m^3]$
Cu	Copper[-]
Cp	Specific heat coefficient$[JK^{-1}Kg^{-1}]$
d	Stretching/shrinking parameter[-]
Da^{-1}	Inverse Darcy number[-]
D	Mass diffusivity$[m^2s^{-1}]$
Ec	Eckert number[-]
$f(\eta)$	Velocity function [-]
h, j, m, n	Constants [-]
K	Permeability of porous medium$[m^2]$
Nr	Radiation[-]
Pr	Prandtl number[-]
qr	Radiative heat flux$[Wm^{-2}]$
Sc	Schmidt number[-]
T_w	Surface Temperature$[K]$
T	Fluid Temperature$[K]$
T_∞	Ambient temperature$[K]$
TiO_2	Titanium dioxide[-]
u, v	velocities $[ms^{-1}]$
u_w	Velocity$[ms^{-1}]$
v_w	Wall velocity$[ms^{-1}]$
x, y	Coordinates$[m]$
Greek symbols	.
β	Solution value[-]
λ	Bingham parameter[-]
η	Similarity variable[-]
Λ	Stefan blowing parameter[-]
Λ	Absorption coefficient$[m^{-1}]$
ψ	Stream function$[m^2s^{-1}]$
σ^*	Stephen Boltzmann constant$\left[Wm^{-2}K^{-4}\right]$
$\theta(\eta)$	Dimension less temperature[-]
$\varphi(\eta)$	Dimension less concentration[-]
Abbreviation	.
B. Cs	Boundary conditions[-]
MHD	Magnetohydrodynamics[-]
hnf	Hybrid nanofluid[-]
nf	Nanofluid[-]
tnf	Ternary nanofluid[-]
ODE	Ordinary Differential Equation[-]
PDE	Partial Differential Equation[-]

focused on using a swirling Al_2O_3 nanofluid jet for heat transfer enhancement on a heated flat plate achieving important increase in the heat transfer when adding nanoparticles. These examples demonstrate that the use of nanofluids in engineering provides endless opportunities.

Radiation is a relevant aspect in thermal engineering, which has not been that studied in the nanofluid literature as deep as convection or conduction. Recently, radiation effects have drawn more attention from researchers in the nanofluid field, mostly because of the many industrial processes in which they are used for. For instance, Saleem et al. [6] examined the thermal radiation and Darcy ratio impact on a Casson fluid flow across a permeable plate by using the Lie Scaling method and showed that the Casson parameter reduces the momentum of the flow. The study in Nazim et al. [7] examined the joule heating impact on the unsteady convective fluid movement across a vertically expanding surface with the impact of the Casson parameter to determine the enhancement in the temperature profile. Saleem et al. [8,9] examined the radiation influence of non-Newtonian fluid movements over the surfaces by utilizing the slip effects and pointed out the strong impact of radiation on the temperature profile. Last but not least, Xu et al. [10] provided a very complete review of radiation with phase variation in nanofluids, revealing that radiation enhances the thermal boundary layer. Porous media has significant use in industrial processes, including solar energy technology, metal thinning, and glass making, which have all been shown to be significantly affected by the radiation effect. In this sense, by taking advantage of the Rosseland approximation, Saleem et al. [11,12] examined the thermal radiation impact on non-Newtonian fluid flows across enhanced porous media that have a reduction in the momentum of fluids. The investigation in Iqbal&Saleem [13] analysed the convective thermal energy transfer of non-Newtonian Casson fluid along a vertical channel and detected that the escalation in the Eckert number strongly influenced the increase in thermal transport, whereas the high Hartmann number retarded the flow velocity. Tufail et al. [14] studied the chemical reaction influence on the magnetic Casson fluid movement across the permeable media and showed that the Casson parameter enhances the heat efficiency of the flow. Tufail et al. [15] investigated the thermal slip impact on the Maxwell fluid movement across the porous shrinking surface by utilizing the Lie group method and pointed out that the Lie group method was better than numerical methods. The impact of Hartmann number, Prandtl, source-sink, radiation and thermal slip parameter on the temperature profile were analysed as well. Also, Mahabaleshwar et al. [16] examined the radiation in the MHD of a nanofluid movement over permeable media in a laminar flow regime and found that the magnetic effect enhances the heat transfer considerably.

The Stefan blowing effect occurs when fluid is ejected from a surface into the surrounding flow, influencing the velocity and pressure distribution near the surface. This effect can enhance momentum transfer and influences heat and mass transfer rates by modifying the boundary layer structure. It is particularly important in applications involving non-Newtonian fluids or nanofluids, where the transport properties behave more complex. By controlling the flow behavior near the surface, the Stefan blowing effect can improve heat dissipation, concentration control, and overall system efficiency in various engineering processes. Its understanding is crucial for optimizing performance in fields like heat exchangers and cooling systems, and it is being vastly studied, as evinced in the literature. In Mahabaleshwar et al. [17], it is described the impact of Schmidt numbers on Newtonian fluids and it was shown that the Schmidt number decays the concentration profiling. The work in Zohra et al. [18] studied a magnetic bio-convectional flow with anisotropic slip effects from a spinning cone, concluding that the skin friction can be increased by modifications in the magnetic field. Alamri et al. [19] analyzed the radiative plane of a convective slip-free Poiseuille nanofluid flow through porous media. Also, Anwar Beg et al. [20] studied a nanofluid from a biomagnetic needle with energy conservation under Stefan blowing, where it was found that all physical quantities decreased when the Stefan blowing was increased and, on the contrary, there was an increase when rising the power law index parameter. Finally, it is worth noting the work by Rana et al. [21], where an investigation of the Lie group investigation of nanofluid slip movement with Stefan blowing impact was carried out, concluding that the diffusion parameter has a key role in retarding the skin friction. Similar aspects were studied in Uddin et al. [22], where similarity equations solved via Chebyshev collocation were used for gyrotactic bioconvection with porous media.

The Schmidt parameter is described as the ratio of kinematic viscosity over molecular diffusion, being thus a parameter to determine mass diffusion in convection processes. Examples of mass diffusion problems in the literature managed through the Schmidt number can be Gromke&Blocken [23] where urban neighborhood air quality was analyzed by means of Reynolds averaged Navier Stokes simulations with turbulent Schmidt number, Calmet&Magnaudet [24] where mass transfer was studied along channel flow with Large Eddy Simulations and high-Schmidt numbers, Gualtieri et al. [25] that explored turbulent Schmidt numbers in environmental flows (a transverse mixing in a shallow water flow, tracer transport in a contact tank, and sediment transport). Also, Mahabaleshwar et al. [26] focused on the impact of the Schmidt number on an Ostwald–de Waele ternary nanofluid over a permeable shrinking sheet to enhance thermal conductivity. The investigation in Fang&Jing [27] explored the combined Stefan-blowing influence from species transfer over a stretched plate in combination with the Stefan blowing effect from species transfer. Sachhin et al. [28] studied the impact of radiation on the pair stress fluid movement across a stretching surface and concluded that radiation has an important role in heat transfer efficiency. Many researchers also studied stretching/shrinking sheets with and without radiation [28–44]. The work in Dawar et al. [45] examined the impact of the magnetic field on squeezing nanofluid flows across rotating channels and found that the magnetic effect reduces the velocity due to the Lorentz force. In addition, [46–48] explored the entropy generation impact on fluid flows across various boundaries. Jawad et al. [49] explored the dissipation impact on the unsteady rotating fluid motion with nonlinear thermal radiation and concluded that dissipation enhances the thermal boundary layer. The study in Salahuddin&Awais [50,51] examined the thermal radiation impact on magnetohydrodynamic fluid flow by solving the equations by the using the Adams-Milne (Predictor–Corrector) technique, to analyse the impact of thermal radiation, viscous dissipation, joule effect, and chemical processes on the flow. Again, Awais& Salahuddin [52,53] studied the thermophysical properties of fluids and nanoparticles across stagnating surfaces and showed that nanoparticles enhance the energy profile. Salahuddin&Awais et al. also carried out related studies of strong interest to this investigation, which can be consulted for further references [54–57]. The investigation in Uddin et al. [58] examined the thermal radiation impact on nanofluid movement along a stretching/shrinking surface with slip conditions, and found out that slip effects reduce the momentum of the fluid flow. The work developed in Beg et al. [59] studied the simulations of magnetohydrodynamics on convective fluid motion with blowing effects, carrying out an extensive parameter impact exploration which included the Stefan blowing effect, nanoparticle concentration, microorganism slips, magnetic number, Lewis number, Falkner-Skan wedge parameter, Peclet number, thermophoresis and Brownian motion. Finally, for further references for the reader, we suggest to see [60–64], whose works include anisotropic slip effects on the fluid flow inside porous media.

Inspired by the abovementioned analysis, the present analysis examined the influence of Stefan blowing, viscous dissipation, and Schmidt number on biviscous Bingham ternary nanofluid movement with heat and concentration over an expanding/shrinking sheet, it is noted that there is a dearth of investigation on Bingham liquids with radiation with permeable media. While prior works have explored individual or limited combinations of these parameters, there remains a clear **research gap** concerning the analytical treatment of Bingham fluids under the simultaneous influence of radiation and flow through a permeable stretching/shrinking medium, plus Stefan blowing effect. The current analysis introduces a special novel contribution by examining the combined influence of blowing effects resulting from substantial species transfer on fluid flow, heat, and mass transport. Thus, the **main novelty of the current investigation** is to provide, for the first time, an analytical solution for the influence of radiation over biviscosity Bingham ternary nanofluid motion with the influence of viscous dissipation and Schmidt number. In this process, heat and mass transfer equations are transformed into ODEs via suitable similarity variables, and the velocity and concentration equations are coupled and calculated simultaneously. Results are discussed with focus on thermal radiation, Stefan blowing parameter, volume fraction, Nusselt number, and Schmidt number, thus developing a valuable investigation on the combined effects of Stefan blowing, Bingham fluid, ternary nanofluid, radiation, porous media, and stretching/shrinking sheet, essential for optimizing thermal management in complex engineering systems. This approach helps to address challenges in heat transfer and fluid flow in industries such as electronics cooling, energy storage, and material processing.

With respect to the practical applications of this study, the combination of the aforementioned effects suggests that such fluids are highly suitable for use in advanced thermal management systems. This includes e.g. applications in cooling of electronics, where precise temperature regulation is needed. Furthermore, the sensitivity of temperature and concentration profiles to Schmidt number and volume fraction parameters provides design-level insights for industrial processes such as catalytic reactors, where diffusion control and efficient energy exchange are crucial. The incorporation of porous media and radiation effects also aligns the study with the requirements of solar energy harvesting systems, insulation technologies, and underground heat storage units. Last but not least, the analytical model developed in this work allows for predictive control of fluid flow and thermal behavior in complex environments and Digital Twins. The strong agreement with previous benchmark studies further reinforces the credibility and applicability of the results, making them a valuable reference for future experimental and industrial research.

The manuscript is broken down into several sections. Section 1 initially introduced the reader to the topic and illustrated an in-depth literature review. Section 2 provides details on the equations that govern the problem. Section 3 shows the analytical solution to the momentum and heat & mass transfer equations, respectively. This section also shows a detailed validation with previous works. Section 4 gives discussion and analysis of the findings from the analytical solution. Finally, Section 5 portrays the conclusions drawn from this investigation. Additionally, in Appendix A the thermophysical properties are provided.

2. Problem specifications and governing equations

This work contains several assumptions, very relevant to carry out the current study. It is important to detail them before introducing the equations and other mathematical or physical explanations. The assumptions taken into account in this work are the following:

- Bi-viscous Bingham fluid model with ternary nanoparticles. We considered such model incorporated into the velocity and temperature formulation. This allows for a more generalized fluid model, but for obvious reasons does not fully capture all non-Newtonian behaviours observed in real industrial fluids with complex rheology.
- Porous medium. The flow is assumed to occur through a porous medium, which introduces additional resistance to the momentum transport. While this aligns with many real-world scenarios such as filtration systems, the properties of the porous structure are idealized, which may limit direct applicability to heterogeneous or anisotropic porous materials, that need special modelling.
- Adding thermal radiation and viscous dissipation in the temperature analysis. The energy equation incorporates thermal radiation and viscous dissipation effects, enhancing the relevance of the model for high-temperature and high-shear applications. However, radiation is modelled in a simplified form, and detailed radiative heat transfer mechanisms are not explicitly resolved.
- Schmidt number in concentration equation. The concentration profile is influenced by the Schmidt number, reflecting mass diffusivity

effects. This is important for modelling species transport, but assumes constant diffusivity, which may vary in practical systems.

- Steady, incompressible, two-dimensional flow. The analysis considers a steady and incompressible flow induced by a shrinking or stretching sheet, neglecting pressure gradients and unsteady effects. This assumption is valid for many controlled or laminar systems, but limits the applicability of the model to transient or compressible flow situations.
- Stretching/shrinking surface. A prescribed surface stretching velocity is assumed, which drives the fluid motion. This velocity must be changed depending on the application.

As said in the description of the assumptions, a bi-viscous Bingham fluid flow with ternary nanoparticles is considered. The rheological equation of the bi-viscosity Bingham fluid was given in [38], defined as:

$$\tau_{ij} = \begin{cases} 2(\mu_B + p_y/\sqrt{2\pi})e_{ij}, \pi > \pi_c, \\ 2(\mu_B + p_y/\sqrt{2\pi_c})e_{ij}, \pi < \pi_c, \end{cases} \tag{1a}$$

with a non-Newtonian yield stressτ_y defined as:

$$P_y = \frac{\mu_B\sqrt{2\pi_c}}{\lambda}, \tag{1b}$$

where πdenotes deformation rate product, product value of bi-viscosity Bingham model is denoted asπ_c, P_y defined as yields stress of the fluid model, and μ_B is denoted as the viscosity of plastic deformation. In Fig. 1 it is shown the sketch of the problem under study, which consists of the bi-viscous Bingham fluid with ternary nanoparticles across a expanding/shrinking surface with a porous medium. The sheet has an imposed boundary condition as moving boundary according to fluid-at-wall velocity$u = ax$, where a is the stretching coefficient, and $x$is the coordinate. Regarding the ternary nanofluid, Table 1 provides thermophysical properties, Fig. 1 presents the sketch of the problem and additional details on the modelling of the ternary nanofluid are given in Appendix A.

According to the assumptions mentioned above, the momentum, temperature, and concentration equations are defined as [1,17,27,38]:

$$\frac{\partial u}{\partial x} + \frac{\partial v}{\partial y} = 0, \tag{2}$$

$$with general form: \nabla\cdot\vec{q} = 0, \tag{2a}$$

Table 1
Thermophysical properties [36–38].

Properties	*SA*	Silver (*Ag*)	Copper (*Cu*)	Titanium Dioxide (TiO_2)
$\rho(kgm^{-3})$	989	10500	8933	4250
$Cp(JkgK^{-1})$	4175	235	385	686.20
$\kappa(WmK^{-1})$	0.6376	429	400	8.9538
$\sigma(S/m)$	2.6×10^{-4}	3.6×10^{7}	59.6×10^{6}	1×10^{-12}

$$u\frac{\partial u}{\partial x} + v\frac{\partial u}{\partial y} = -\frac{1}{\rho_{tnf}}\frac{\partial p}{\partial x} + \frac{\mu_{tnf}}{\rho_{tnf}}\left(1+\frac{1}{\lambda}\right)\frac{\partial^2 u}{\partial y^2} - \frac{\mu_{tnf}}{\rho_{tnf}}\left(1+\frac{1}{\lambda}\right)\frac{1}{K}u, \tag{3}$$

$$u\frac{\partial v}{\partial x} + v\frac{\partial v}{\partial y} = -\frac{1}{\rho_{tnf}}\frac{\partial p}{\partial y} + \frac{\mu_{tnf}}{\rho_{tnf}}\left(1+\frac{1}{\lambda}\right)\frac{\partial^2 v}{\partial y^2} - \frac{\mu_{tnf}}{\rho_{tnf}}\left(1+\frac{1}{\lambda}\right)\frac{1}{K}v, \tag{4}$$

$$with general form: [(\vec{q}\cdot\nabla)\vec{q}] = -\frac{1}{\rho_{tnf}}\nabla p + \frac{\mu_{tnf}}{\rho_{tnf}}\left(1+\frac{1}{\lambda}\right)\nabla^2\vec{q} - \left(1+\frac{1}{\lambda}\right)\frac{\nu_{tnf}}{K}\vec{q}, \tag{4a}$$

$$u\frac{\partial T}{\partial x} + v\frac{\partial T}{\partial y} = \frac{\kappa_{tnf}}{(\rho Cp)_{tnf}}\frac{\partial^2 T}{\partial y^2} - \frac{1}{(\rho Cp)_{tnf}}\frac{\partial qr}{\partial y} + \frac{\mu_{tnf}}{(\rho Cp)_{tnf}}\left(1+\frac{1}{\lambda}\right)\left(\frac{\partial u}{\partial y}\right)^2, \tag{5}$$

$$with general form: (\rho Cp)_{tnf}[(\vec{q}\cdot\nabla)T] = \kappa_{tnf}\nabla^2 T - \nabla qr + \mu_{tnf}\left(1+\frac{1}{\lambda}\right)(\nabla\vec{q})^2, \tag{5b}$$

and finally,

$$u\frac{\partial C}{\partial x} + v\frac{\partial C}{\partial y} = D\left(\frac{\partial^2 C}{\partial y^2}\right). \tag{6}$$

$$with general form: [(\vec{q}\cdot\nabla)C] = D\,\nabla^2 C, \tag{6b}$$

where u and v are taken as the velocities of x and y, C stands for species concentration, T stands for temperature, ρ stands for density, $\vec{q} = (u,v)$is the velocity vector, μ stands for dynamic viscosity, D stands for mass diffusivity co-efficient, K is the permeability coefficient, Cp stands for constant pressure specific heat capacitance. The boundary conditions of the partial differential equations (PDEs) are defined as [17,27,38]:

$$\left.\begin{array}{l} u = u_w(x) = ax, \quad v = v_w, \quad T = T_w, \quad C = C_w \quad \text{at} \quad y = 0, \\ u \to 0, \qquad\qquad T \to T_\infty, \quad C \to C_\infty, \quad \text{as} \quad y \to \infty, \end{array}\right\}, \tag{7}$$

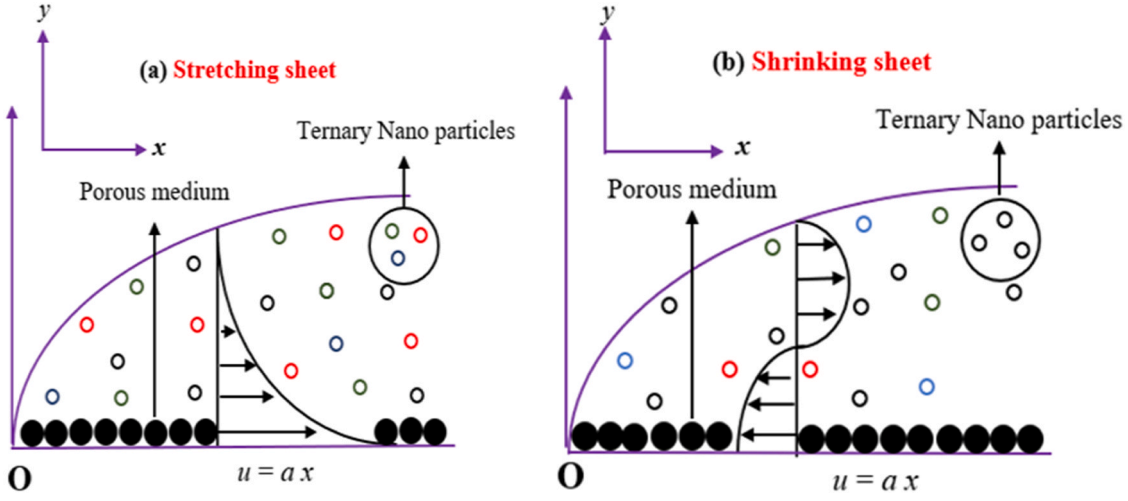

Fig. 1. Sketch of the problem. Figure made by the authors.

where the subscript w refers to the quantities at the wall (sheet). Radiation is modelled according to the well-known Rosseland approximation [1,4,38]:

$$qr = -\frac{4\sigma*}{3k*}\frac{\partial T^4}{\partial y}, \tag{8}$$

where $\sigma*$denotes the Stefan-Boltzmann constant, $k*$stands for absorption. If it is assumed that the heat variation inside the fluid flow is comparatively small, by taking advantage of a Taylor expansion with truncated greater order terms, one can approximate:

$$T^4 \cong 4T_\infty^3 - 3T_\infty^4, \tag{9}$$

by using Eqs. (8) and (9) get the following form,

$$\frac{\partial qr}{\partial y} = -\frac{16\sigma * T_\infty^3}{3k*}\frac{\partial^2 T}{\partial y^2}, \tag{10}$$

and by combining this Eq. (10) with Eq. (5), one can obtain:

$$u\frac{\partial T}{\partial x} + v\frac{\partial T}{\partial y} = \frac{\kappa_{tnf}}{(\rho Cp)_{tnf}}\frac{\partial^2 T}{\partial y^2} + \frac{1}{(\rho Cp)_{tnf}}\frac{16\sigma * T_\infty^3}{3k*}\frac{\partial^2 T}{\partial y^2} + \frac{\mu_{tnf}}{(\rho Cp)_{tnf}}\left(1+\frac{1}{\lambda}\right)\left(\frac{\partial u}{\partial y}\right)^2. \tag{11}$$

This equation agglutinates the thermal term of the system. For the ease of analytically solving the system of PDEs, similarity variables are defined to solve Eqs. (2) - (6). By following the steps of previous works [17,27,38], we thus obtain:

$$\left.\begin{aligned} &\psi = (\sqrt{a\nu})x\,f(\eta), && \eta = \sqrt{\frac{a}{\nu}}y,\\ &u = axf_\eta(\eta), && v = -\sqrt{a\nu}f(\eta),\\ &\varphi(\eta) = \frac{C-C_\infty}{C_w-C_\infty}, && \theta(\eta) = \frac{T-T_\infty}{T_w-T_\infty}, \end{aligned}\right\} \tag{12}$$

Also, the stream function ψ is classically described by means of

$$u = \frac{\partial \psi}{\partial y} \quad \text{and} v = -\frac{\partial \psi}{\partial x}. \tag{13}$$

A similar approach to the works in [34] and [35] is followed here. By Eq. (4) and the boundary conditions defined in Eq. (7), one can obtain

$$P = P_0 - \rho\frac{v^2}{2} + \mu\frac{\partial v}{\partial y} - C_1 = 0. \tag{13a}$$

whereC_1 is a constant. Finally, after applying the similarity calculations to the given governing Eqs. (3)-(6), the system of PDEs is transformed into:

$$\left(1+\frac{1}{\lambda}\right)A_1 f_{\eta\eta\eta}(\eta) - A_1\left(1+\frac{1}{\lambda}\right)Da^{-1}f_\eta(\eta) - A_2\left[f_\eta(\eta)^2 - f(\eta)f_{\eta\eta}(\eta)\right] = 0, \tag{14}$$

$$(A_3+Nr)\theta_{\eta\eta}(\eta) + A_4\Pr f(\eta)\theta_\eta(\eta) + A_1\Pr Ec\left(1+\frac{1}{\lambda}\right)(f_{\eta\eta}(\eta))^2 = 0, \tag{15}$$

$$\varphi_{\eta\eta}(\eta) + Sc\,f(\eta)\varphi_\eta(\eta) = 0. \tag{16}$$

The constants appearing in the equations above are basically the following ratios:

$$A_1 = \frac{\mu_{tnf}}{\mu_f}, A_2 = \frac{\rho_{tnf}}{\rho_f}, A_3 = \frac{\kappa_{tnf}}{\kappa_f}, A_4 = \frac{(\rho Cp)_{tnf}}{(\rho Cp)_f}.$$

In order to have consistency in the calculation, the boundary conditions must be also transformed. Thus, the modified boundary conditions for the Eqs. (14)-(16) result in [17,27,38]:

$$\left.\begin{aligned} &f(0) = \Lambda(\varphi_\eta)_{\eta=0},\ f_\eta(0) = d,\ \theta(0) = 1, \varphi(0) = 1, \text{as}\eta\to 0,\\ &f_\eta(\infty)\to 0,\ \theta(\infty)\to 0,\ \varphi(\infty)\to 0, \text{at}\eta\to\infty, \end{aligned}\right\} \tag{17}$$

To assess the effects when varying certain parameters, dimensionless numbers allow to compare and analyse results in fluid mechanics at any scale. These numbers control the characteristics of the numerical, analytical, or physical experiment. The dimensionless number used in the present investigation are listed below:

- $Ec = \frac{u_w^2}{Cp(T_w - T_\infty)}$, is the Eckert number,
- $Nr = \frac{16\sigma * T_\infty^3}{3k*\kappa_f}$, denotes the thermal radiation,
- $\Pr = \frac{\nu}{\alpha}$, denotes the Prandtl number,
- $Sc = \frac{\nu}{D}$, denotes the Schmidt number,
- $Da^{-1} = \frac{\nu}{K\,a}$, denotes the inversed Darcy number,
- Λ, denotes the Stefan blowing parameter, leading to a velocity given as $v_w = -(\sqrt{a\nu})\Lambda\varphi_\eta(0)$.

3. Analytical solution to the problem

The analytical solution for the transformed momentum Eq. (14) is given by [17,27]

$$f(\eta) = \frac{A_1\left(1+\frac{1}{\lambda}\right)Da^{-1} - A_1\left(1+\frac{1}{\lambda}\right)\beta^2}{A_2\beta} - \frac{d}{\beta}e^{(-\beta\eta)}, \rightarrow where \beta > 0 \tag{18}$$

Also, by substituting Eq. (18) into Eqs. (15) and (16), and by using the transformed variables $t = \frac{\Pr}{\beta^2}\exp(-\beta\eta)$ and$\xi = \frac{Sc}{\beta^2}\exp(-\beta\eta)$, the heat and mass transfer equations are converted into:

$$t\frac{d^2\theta}{dt^2} + (1-m+nt)\frac{d\theta}{dt} = \frac{A_1 Ec\left(1+\frac{1}{\lambda}\right)\beta^2 d}{\Pr*}t, \tag{19}$$

$$\xi\frac{d^2\varphi}{d\xi^2} + (1-h+j\xi)\frac{d\varphi}{d\xi} = 0, \tag{20}$$

where we have defined the parameters m, n, j, Pr^* and h as:

$$m = \frac{A_4\Pr\left[A_1\left(1+\frac{1}{\lambda}\right)Da^{-1} - A_1\left(1+\frac{1}{\lambda}\right)\beta^2\right]}{A_2\beta^2(A_3+Nr)},$$
$$n = \frac{dA_4}{(A_3+Nr)}, j = d, \Pr* = \frac{\Pr}{\beta^2}. \tag{21}$$
$$h = \frac{Sc\left[A_1\left(1+\frac{1}{\lambda}\right)Da^{-1} - A_1\left(1+\frac{1}{\lambda}\right)\beta^2\right]}{A_2\beta^2}$$

and the converted equations are subject to the modified boundary conditions:

$$\left.\begin{aligned} &\varphi\left(\frac{Sc}{\beta^2}\right) = 1, \varphi(0) = 0, \theta\left(\frac{\Pr}{\beta^2}\right) = 1, \theta(0) = 0, \end{aligned}\right\} \tag{22}$$

Now the Frobenius method can be applied to obtain the solution as infinite series, thus defining the derivatives for Eq. (19):

$$\theta(t) = \sum_{r=0}^{\infty} a_r t^{r+k}, \tag{23}$$

$$\theta_\eta(t) = \sum_{r=0}^{\infty} a_r(r+k)t^{r+k-1}, \tag{24}$$

$$\theta_{\eta\eta}(t) = \sum_{r=0}^{\infty} a_r(r+k)(r+k-1)t^{r+k-2}. \tag{25}$$

Following this approach, the final solution after transformation of

Eq. (19) yields

$$\theta(\eta) = \frac{(e^{-\beta\eta})^m(1-\xi_1)\text{Hypergeometric}\left[m,\quad 1-m,\quad n\frac{\text{Pr}}{\beta^2}e^{-\beta\eta}\right]}{\text{Hypergeometric}\left[m,\quad 1-m,\quad n\frac{\text{Pr}}{\beta^2}\right]} + \xi_1 t. \tag{26}$$

where $\xi_1 = \frac{A_1 Ec\left(1+\frac{1}{\lambda}\right)}{\text{Pr}_*}$ is a constant.

The Nusselt number, which represents the amount of heat transfer in the exchange between a solid and a fluid due to convection, according to [4,49] can be calculated by

$$Nu = \frac{xq_w}{\kappa_f(T_w - T_\infty)} \Rightarrow \frac{Nu}{\sqrt{\text{Re}_x}} = -(A_3 + Nr)\theta'(0), \tag{27}$$

where $\text{Re}_x = \frac{a\,x^2}{\nu_f}$ is local Reynolds number. To solve the heat flux on the sheet one can simply apply the Fourier equation plus the Rosseland approximation for the radiation. That is to say,

$$q_w = -\left[\left(\kappa_{tnf} + \frac{16\sigma_* T_\infty^3}{3k_*}\right)\left(\frac{\partial T}{\partial y}\right)_{y=0}\right],$$

$$\left[\frac{A_1 Da^{-1} - \left(1+\frac{1}{\lambda}\right)A_1\beta}{A_2} - \frac{d}{\beta}\right] = \Lambda\left[-\beta + \frac{h\,j\,Sc\ \text{Hypergeometric}\left[1+h,\quad 2-h,\quad j\frac{Sc}{\beta^2}\right]}{\text{Hypergeometric}\left[h,\quad 1-h,\quad j\frac{Sc}{\beta^2}\right]}\right]. \tag{35}$$

Again, the solution for concentration Eq. (20) can be calculated by applying the Frobenius method as follows:

$$\varphi(\xi) = \sum_{r=0}^{\infty} a_r \xi^{r+k}, \tag{28}$$

$$\varphi_\eta(\xi) = \sum_{r=0}^{\infty} a_r (r+k)\xi^{r+k-1}, \tag{29}$$

$$\varphi_{\eta\eta}(\xi) = \sum_{r=0}^{\infty} a_r (r+k)(r+k-1)\xi^{r+k-2}. \tag{30}$$

The final solution to Eq. (20) is thus

$$\varphi(\eta) = \frac{(e^{-\beta\eta})^h \text{Hypergeometric}\left[h,\quad 1-h,\quad j\frac{Sc}{\beta^2}e^{-\beta\eta}\right]}{\text{Hypergeometric}\left[h,\quad 1-h,\quad j\frac{\text{Pr}}{\beta^2}\right]}. \tag{31}$$

By differentiating the above Eq. (31) and by taking $\eta\to 0$, the first derivative $(\phi_\eta(\eta))_{\eta=0}$ yields:

$$\varphi_\eta(\eta) = \frac{\left\{e^{-2\beta\eta}\left[\begin{array}{l} e^{-\beta\eta}(m-1)\beta^2\,\text{Hypergeometric}\left[h,\quad 1-h,\quad e^{-\beta\eta}\frac{Sc}{\beta^2}j\right] + \\ hj\,Sc\,\text{Hypergeometric}\left[1+h,\quad 2-h,\quad e^{-\beta\eta}\frac{Sc}{\beta^2}j\right]\end{array}\right]\right\}}{(h-1)\beta\ \text{Hypergeometric}\left[h,\quad 1-h,\quad \frac{Sc}{\beta^2}j\right]}, \tag{32}$$

$$\varphi_\eta(0) = -\beta + \frac{h\,j\,Sc\ \text{Hypergeometric}\left[1+h,\quad 2-h,\quad \frac{Sc}{\beta^2}j\right]}{\text{Hypergeometric}\left[h,\quad 1-h,\quad \frac{Sc}{\beta^2}j\right]}. \tag{33}$$

By using Eq. (18) we can calculate the undefined β thanks to the boundary condition

$$f(0) = \Lambda(\varphi_\eta(\eta))_{\eta=0}. \tag{34}$$

Finally, by combining Eqs. (18), (33) and (34), the first derivative for concentration regarding the Blasius similarity variable is obtained as:

In order to provide a more accessible explanation to the reader, we break down the main phases to reproduce the obtention of the exact solution in the following:

- The governing Eqs. (2) - (6) are transformed to nonlinear ODEs using similarity terms.
- The transformed differential Eqs. (14 – 16) with boundary conditions (7) are calculated by the exact method.
- Using modified boundary conditions (17), can be solved the solution for the velocity equation by using coupled boundary conditions.
- The Nusselt number is then calculated by using Eq. 27.
- By utilizing new terms $t = \frac{\text{Pr}}{\beta^2}e^{-\beta\eta}$ and $\xi = \frac{Sc}{\beta^2}e^{-\beta\eta}$, it is calculated the energy and concentration equations and gained Eqs. (15) and (16). By using Hypergeometric functions, can be obtained the solutions for temperature and concentration equations.
- Solution β is calculated by boundary condition (17) with support from Eq. (34), by using Eqs. (18) and (33).

3.1. Validation of the analytical solution. Comparison of the current solution to related works in the literature with limit test case scenarios

A proper validation first is important to trust the results from this work, even though the calculations are analytical. The solution obtained

Table 2
Comparing the choices of β for various choices of Sc and Λ for $\lambda\to\infty, Da^{-1} = 0, Nr = 0, \phi = 0, Ec = 0$.

	$\Lambda = 5$, Fang&Jing [27]	Present results	$\Lambda = 10$, Fang&Jing [27]	Present results	$\Lambda = 20$, Fang&Jing [27]	Present results	$\Lambda = 30$, Fang&Jing [27]	Present results
$Sc = 0.1$	0.8338	0.82261	0.7362	0.75622	0.6226	0.65623	0.5562	0.58338
$Sc = 1$	0.6608	0.64388	0.5970	0.51735	0.5438	0.51732	0.5173	0.56608
$Sc = 10$	0.7472	0.70268	0.7236	0.69135	0.7026	0.79132	0.6913	0.67472
$Sc = 100$	0.8716	0.85591	0.8635	0.85172	0.8559	0.85173	0.8517	0.88716

Table 3
Comparing the choices of $-\varphi'(0)$ for various choices of Sc and $\Lambda$for $\lambda\to\infty, Da^{-1}=0, Nr=0, \phi=0, Ec=0$.

	$\Lambda=2$, Fang&Jing [27]	Present results	$\Lambda=4$, Fang&Jing [27]	Present results	$\Lambda=6$, Fang&Jing [27]	Present results	$\Lambda=8$, Fang&Jing [27]	Present results
$Sc=0.1$	0.0827	0.07562	0.0760	0.07562	0.0705	0.05623	0.0660	0.05833
$Sc=1$	0.2807	0.21734	0.1949	0.11735	0.1520	0.15732	0.1257	0.16608
$Sc=10$	0.2469	0.29135	0.1421	0.19135	0.1016	0.09132	0.0797	0.07472
$Sc=100$	0.1244	0.15172	0.0673	0.05172	0.0468	0.05173	0.0361	0.028716

Table 4
Comparing the values of $-\theta'(0)$ for various values of Sc and ΛforPr $=10$, $\lambda\to\infty, Da^{-1}=0, Nr=0, \phi=0, Ec=0$.

	$\Lambda=2$, Fang&Jing [27]	Present results	$\Lambda=4$, Fang&Jing [27]	Present results	$\Lambda=6$, Fang&Jing [27]	Present results	$\Lambda=8$, Fang&Jing [27]	Present results
$Sc=0.1$	1.3487	1.07562	0.7464	0.75621	0.3900	0.39623	0.1930	0.09833
$Sc=1$	0.1503	0.21734	0.0192	0.01735	0.0038	0.00732	0.0010	0.00608
$Sc=10$	0.2469	0.29135	0.1421	0.14135	0.1016	0.19132	0.0797	0.07472
$Sc=100$	0.9624	0.95172	0.8781	0.85172	0.8331	0.85173	0.8030	0.82871

Table 5
Comparison with associated analytical works.

Previous Works by	Fluids	Solutions of Velocity equations
Crane 1970 [40]	Newtonian	$\beta=1,$
Pavlov 1974 [41]	Newtonian	$\beta=\sqrt{1+M},$
Umair [42]	Non-Newtonian	$f(\eta)=f_w+\frac{\lambda}{\beta}(1-\exp[-\beta\eta]),$ $\beta=\frac{3f_w\left(\frac{\rho_{hnf}}{\rho_f}\right)\pm\sqrt{9f_w^2\left(\frac{\rho_{hnf}}{\rho_f}\right)^2+4\left(\frac{\mu_{hnf}}{\mu_f}\right)3\lambda\left(\frac{\rho_{hnf}}{\rho_f}\right)+\left(\frac{\sigma_{hnf}}{\sigma_f}\right)M}}{2\left(\frac{\mu_{hnf}}{\mu_f}\right)},$
Turkyilmazoglu [43]	Newtonian	$f(\eta)=s-\frac{1-e^{-\beta\eta}}{\beta},$ $\beta=\frac{s\pm\sqrt{-4-2K+s^2}}{2+K}.$
Usafzai [44]	Newtonian	$f(\eta)=s+a\frac{1-e^{-\beta\eta}}{\beta+b\beta^2},$ $(2+R)b\beta^3+(2+R-2sb)\beta^2-2s\beta-2a=0.$
Present work	Non-Newtonian	$f(\eta)=\frac{A_1Da^{-1}-A_1\left(1+\frac{1}{\lambda}\right)\beta^2}{A_2\beta}-\frac{d}{\beta}e^{(-\beta\eta)},$ where$\beta>0.$

by using similarity transformations is validated in this subsection with previous works in the literature, concretely with Fang&Jing [27] in Tables 2, 3 and 4. In these three tables, our model was adapted to the Fang&Jing [27] case scenario (heat and mass transfer across an expanding sheet with Stefan blowing impact of mass transfer under high flux conditions) by removing the porous media behaviour (permeability zero, i.e. $Da^{-1}=0$), modelling the sheet as stretching ($d=1$), low velocity (laminar flow) over boundary layer Eckert number ($Ec=0$), no thermal radiation ($Nr=0$), and Newtonian viscous flow (Bingham parameter $\lambda\to\infty$). The comparison for validation reveals that the solution of our model matches very well Fang&Jing [27] results and the model seems to predict accurately the flow behaviour. Amongst the compared parameters, $-\theta'(0)$ seems to exhibit the larger discrepancies, but still very close to the Fang & Jing's results. Finally, in Table 5 it is shown a summary table for a comparison for the reader with other works in the literature that solved the momentum equation too in other scenarios.

3.2. Numerical validation

For an extended numerical validation, it has been used the Runge-Kutta technique to calculate the governing equations to ODEs, introducing new variables to transform greater ODEs. That is to say:

$$y_1=f,\ y_2=f',\ y_3=f'',\ y_4=\theta,\ y_5=\theta',\ y_6=\varphi,\ y_7=\varphi'. \tag{36}$$

Thus, following these steps, the governing ODEs (14) – (16) are as follows

$$\begin{aligned}
&y_2^1=y_3,\ y_3^1=-\left(\left(\frac{1}{A_1\left(1+\lambda^{-1}\right)}\right)\left(A_2y_1y_3-A_2y_2^2-A_1\left(1+\lambda^{-1}\right)Da^{-1}y_2\right)\right),\\
&y_4^1=y_5,\ y_5^1=-\left(\left(\frac{1}{(A_3+Nr)}\right)\left(\mathrm{Pr}A_4y_1y_5+A_1\mathrm{Pr}Ec\left(1+\lambda^{-1}\right)(y_2)^2\right)\right),\\
&y_6^1=y_7,\ y'_7=-\left(Scy_1y_7\right),
\end{aligned} \tag{37}$$

By taking $\phi=0, Nr=0, Ec=0$. The findings for the reduced Nusselt number $-\theta'(0)$are assessed by Khan [63], Wang [64] for various values of Prandtl number in Table 6. In the comparison we can see that there is good agreement between the comparison for every Prandtl number value, revealing a highly accuracy in the solution.

4. Results and discussion

The influence of parameter variations in the investigation of the Stefan blowing and Schmidt number on bi-viscous Bingham ternary

Table 6
Comparison of reduced Nusselt number $-\theta'(0)$values for Prandtl number while taking $\phi=0$, $Nr=0$, $Ec=0$.

Pr	Khan [63]	Wang [64]	Present results
0.07	0.6630	0.6056	0.609872
0.20	0.1691	0.1691	0.169223
0.70	0.4539	0.4539	0.453133
2.00	0.9113	0.9114	0.911002
7.00	1.8954	1.8954	1.895284
20.00	3.3539	3.3539	3.353911
70.00	6.4622	6.4622	6.462222

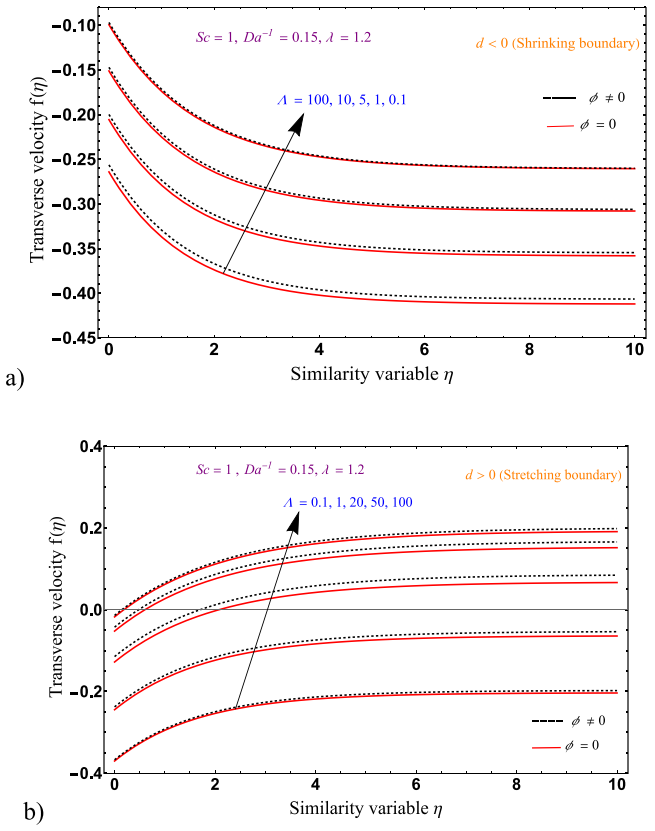

Fig. 2. Evolution of the transverse velocity for different Stefan blowing parameters for a)shrinking boundary and b) stretching boundary.

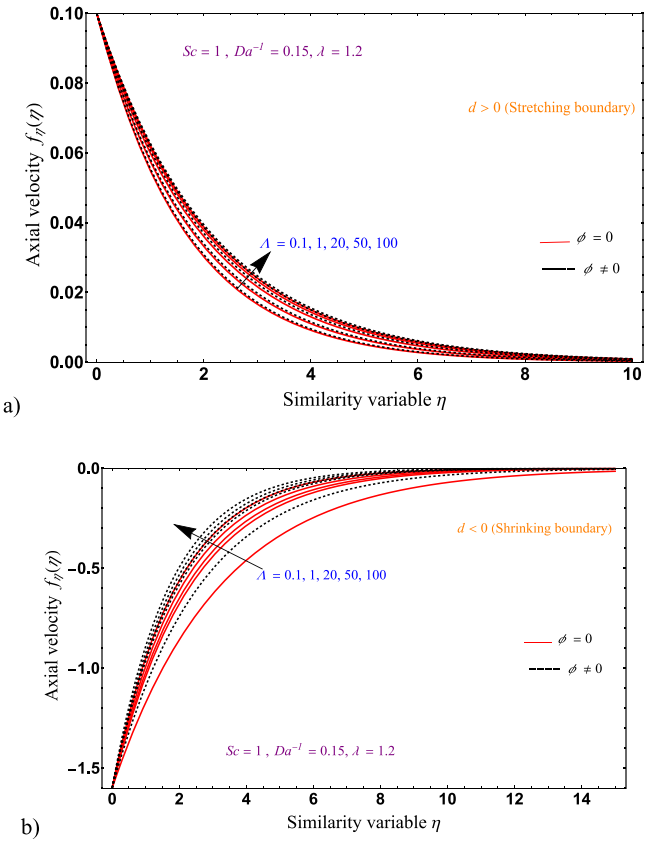

Fig. 3. Evolution of the axial velocity for different Stefan blowing parameters for a) stretching boundary and b) shrinking boundary.

nanofluid flow, heat, and concentrations is studied in this section. The extensive parameter exploration developed in this section allows to have a deeper understanding of the physics behind this nanofluid under the described conditions, of prior importance in the development of any further engineering applications.

In Fig. 2 the transverse velocity is represented for various choices of Stefan blowing parameter (Λ = 0.1, 1, 20, 50, and 100) for both stretching and shrinking boundaries. Also, an inverse Darcy number of $Da^{-1} = 0.15$, Bingham parameter of $\lambda = 1.2$, and Schmidt number of unities $Sc = 1$, are taken as problem conditions. These parameters are chosen so for a proper order of comparison with Fang&Jing [27], where one can find similar values for the Darcy, Schmidt, Bingham and Stefan blowing parameters, although their flow is Newtonian single-phase (viscous flow without nanoparticles, $\phi = 0$, and only constrained by a stretching boundary). It is now observed that, when considering a ternary fluid with nanoparticles, the transverse velocity is slightly increased with respect to the original monophasic viscous flow considered in Fang&Jing [27], and this increment is more notorious for the greater choices of the Stefan blowing term. The increase in velocity seems to be mainly a consequence of the Bingham parameter, since its growth reduces the fluid stress, facilitating the ternary Bingham fluid to flow. In addition, one must recall that for this type of problem, the velocity and concentration fields are coupled, since the mass blowing effect is linked to concentration, so hence the reasonable strong impact of the Stefan blowing parameter, as already discussed in Fang&Jing [27]. Moreover, it is noted that for a shrinking surface, to increase the Stefan blowing term diminishes the transverse velocity, whereas for a stretching boundary, the transverse velocity increases.

In Fig. 3 the axial velocity is analysed for the same inverse Darcy, Schmidt, Bingham and Stefan blowing parameters as in Fig. 2. In Fig. 3, again the impact of the nanoparticles is a very gentle increase on the (axial) velocity, as seen for the expanding sheet (Fig. 3(a)), and more impactful on the shrinking sheet (Fig. 3(b)). The same occurs for the sensitivity to the Stefan blowing parameter, being more sensitive in the shrinking case. Also, the trend of the axial velocity is different depending on the stretching or shrinking nature of the wall sheet, faster approaching to zero in the stretching case (around $\eta = 10$). Thus, we can conclude that, in terms of the velocity field, it is more relevant the parameter setting for shrinking sheets. Physically, it represents the rate at which mass is added or extracted from the fluid at the boundary, which influences fluid motion near the sheet. A higher Stefan blowing parameter typically increases the fluid velocity near the sheet because it indicates a higher rate of mass injection, which helps to accelerate the flow. On the contrary, a lower Stefan blowing parameter can lead to a decrease in velocity, as less mass is introduced, thus reducing the overall momentum of the fluid. This parameter is essential for controlling the behaviour of nanofluids in applications such as cooling systems, where the manipulation of flow velocity can optimize heat transfer and overall system efficiency.

Fig. 4 shows the wall concentration gradient ($-\varphi_\eta(0)$) dependent on β, when varying the Schmidt number from 0.1 to 0.5, with Bingham parameter taken as 1.2, and inverse Darcy number as unity. For the shrinking boundary, Fig. 4(a), the differences between $\phi = 0$ and $\phi \neq 0$are very remarkable. When nanoparticles are added to the flow with $\phi = 0.01$, there are high-concentration gradients as seen by asymptotic-like curves near $\beta = 0$ (which make sense, since it appears in the denominator of the equation); and then, when increasing β, the wall concentration gradient grows. However, for a fluid without nanoparticles, there is no asymptotic-like behaviour, and the concentration tends to zero for $\beta \to 0$. For the different Schmidt numbers, the nanofluid performance is smooth and predictable, whereas the $\phi = 0$ fluid has some overlaps around $\beta = 1$. For both cases, after $\beta = 1$ the behaviour is very linear.

Fig. 4(b) shows that, for a stretching sheet, the behaviour is nearly

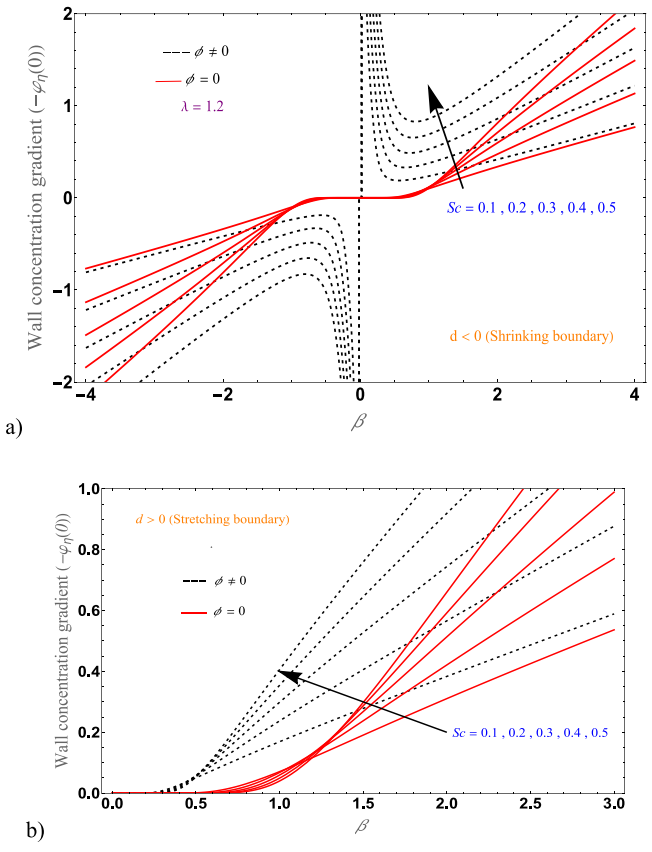

Fig. 4. Evolution of the wall concentration gradient with β for different Schmidt numbers in a) a shrinking boundary and b) a stretching boundary.

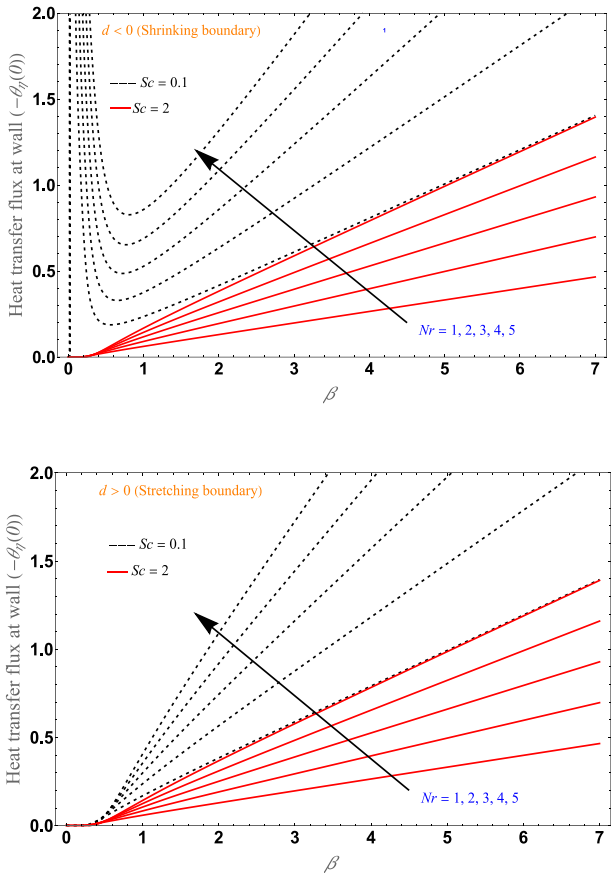

Fig. 5. Evolution of the heat transfer flux at wall with β for different thermal radiation numbers in a) a shrinking boundary and b) a stretching boundary.

the same as for the shrinking sheet in a fluid without nanoparticles. However, when ternary nanoparticles are added for a Bingham fluid with $\phi = 0.01$, there is a similar behaviour to the base fluid alone, but at lower values of β. This time, no asymptotic-like behaviour is observed for $\beta \to 0$. At this point, the wall concentration gradient is zero.

In Fig. 5 it is shown the evolution of the heat transfer flux with β, by considering variations in the thermal radiation parameter, under a $\phi = 0.01$ fluid, two configurations with Sc values of 0.1 and 2, respectively, and the thermal radiation parameter is varied as 1, 2, 3, 4 and 5. It is observed in the impact of Nr that, when increasing the thermal radiation number, the heat transfer at wall is also increased. This is an obvious result, which reveals that the equations provide reasonable results. Physically, the Schmidt number impacts on how quickly species are transported relative to the momentum in the fluid. A greater Schmidt parameter evinces that mass diffusion is slower than momentum diffusion, tending to a steeper concentration gradient near the wall, as the species have less tendency to spread out. In contrast, a lower Schmidt number implies faster mass diffusion, which results in a less steep concentration gradient. This parameter is essential in processes such as chemical reactions or heat transfer applications, where controlling the concentration near the surface can significantly influence the efficiency and behaviour of the system.

Fig. 6 displays the relationship between the Stefan blowing term, Λ, and Schmidt number, Sc, with respect to the stretching/shrinking parameter (Fig. 6(a)), and with respect to the inverse Darcy number (Fig. 6(b)). In both figures, $\phi = 0 \text{and} \phi \neq 0$(equals to 0.01) cases are studied. In Fig. 6(a) can be observed that in the Stefan blowing parameter representation, for ϕ choice 0.01, the curves of d start from zero, while for ϕ of zero value, the plots of d start from unity, but with identical behaviour. This means that when $\phi \neq 0$, the Stefan blowing parameter is much lower than when $\phi = 0$, for the same stretching/shrinking parameter d. Very similar behaviour is found in Fig. 6(b), where the Stefan blowing parameter is represented with respect to the inverse Darcy number over for a stretching boundary. In this plot, it can be seen the behaviour at Darcy equals zero (non-porous) the Stefan blowing for $\phi \neq 0$ is zero, i.e., there is no blowing nor suction, and it is then exponentially growing with the inverse Darcy number. It is remarkable that the Stefan blowing term is always greater than zero in Fig. 6, meaning that there is mass blowing at the wall, and no suction (suction appears when the parameter is lower than zero) [27].

Fig. 7 displays one of the most relevant plots of this work, which is the relationship between the Stefan blowing effect and β. Their mutual influence is very relevant because this provides additional understanding on the behaviour of the velocity profiles, as already discussed in Fang&Jing [27]. The results of their work are reproduced here in Fig. 7 for $\phi = 0$, obtaining identical results in the trend in the $\Lambda(\beta)$ plot for different Sc numbers. In the present investigation, when considering the $\phi \neq 0$, with actual value $\phi = 0.01$, differences are only noticed at low values of β, what actually corresponds to $\Lambda = 0$ values. In general, it is concluded from the plot that when $\phi \neq 0$, the Stefan blowing term is low if β is low too. And the observed trend (as also observed in [27]) is that when Λ increases, β decreases, especially for low values of the Schmidt number (mass diffusion more notorious than momentum diffusion). This is the reason in Figs. 2 and 3 of having a notable degree of variation in the velocity profiles when varying the Stefan blowing term, and a large variation in concentration gradient in Fig. 4 when varying the Schmidt. In other words, when $\Lambda > 0$, the value of β was varied and, thus, the decay of velocity profiles. Regarding the concentration gradient shown in Fig. 4 (recall the concentration problem is coupled with the velocity problem), the variation in the Schmidt number dramatically affected the Λ and β, thus producing important variations in the behaviour of the concentration.

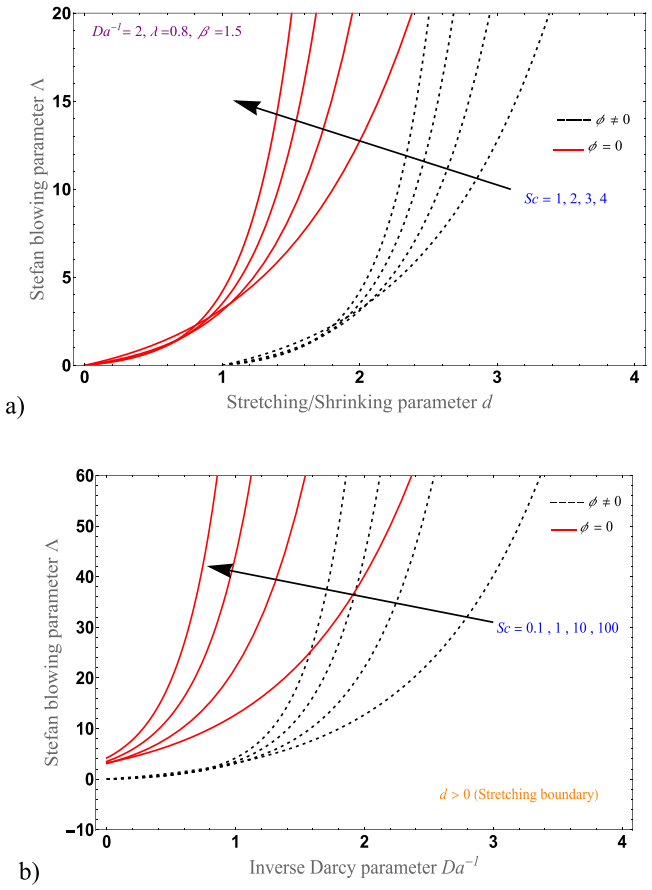

Fig. 6. Stefan blowing parameter for different Schmidt numbers with respect to a) the stretching/shrinking parameter and b) inverse Darcy number.

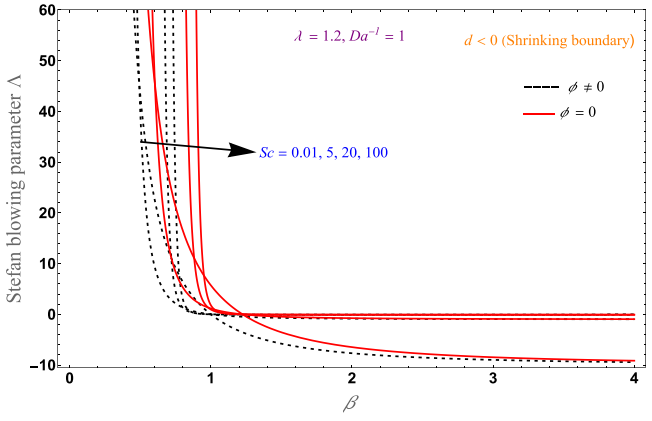

Fig. 7. Relationship of the Stefan blowing effect withβ at different Schmidt numbers.

The study of the distribution of the temperature is also very relevant and will be analysed in the upcoming plots. Fig. 8 illustrates the impact of *Sc* on temperature distribution in regard to η with the stretching boundary ($d > 0$), Prandtl number of 6.72, radiation number equals to 2, *Ec* of 0.5, and Bingham parameter of 1.2. The Schmidt (*Sc*) is varied from 1 to 4 and, as expected, it is observed an increase in the temperature distribution when increasing *Sc* and when $\phi \neq 0$. The ternary nanoparticles increase the heat transfer performance of the movement, and the variation in the Schmidt number evinces that mass diffusion in fluids grows with the temperature and is inversely proportional to the viscosity variation with heat, so *Sc* increments the temperature evolution, which

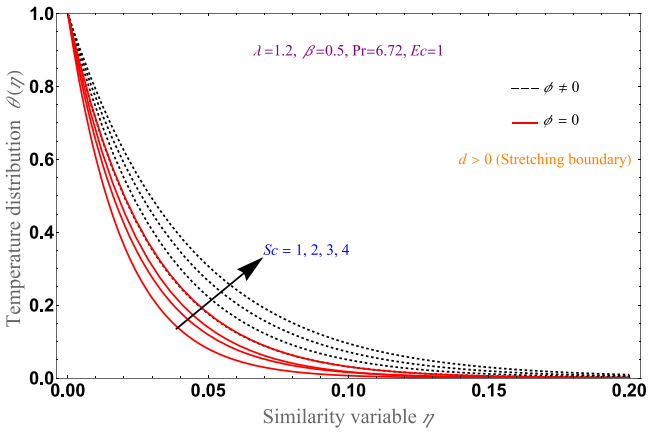

Fig. 8. Temperature distribution over the similarity variable for variations of *Sc* parameter.

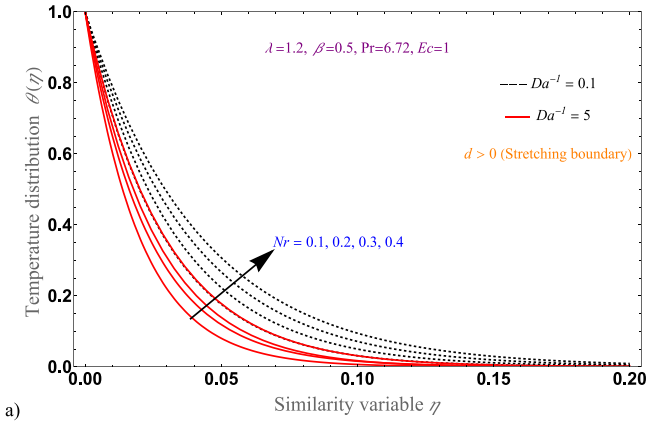

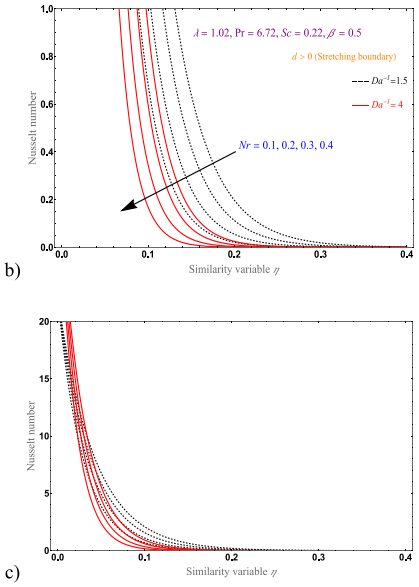

Fig. 9. Evolution with the similarity parameter when varying *Nr* for: a) temperature, and Nusselt number in zoom (b) and global view (c).

together with the stretching effect, enlarges the thermal boundary layer.

Fig. 9 portrays the temperature and Nusselt number distributions, when varying the thermal radiation parameter, in the same scenario described for Fig. 8. Fig. 9(a), which shows the temperature distribution when varying *Nr*, yields almost the same behaviour as when the *Sc* was

varied, since an increase in *Nr* is evidently increasing temperature with higher values of temperature when $\phi \neq 0$. However, in Fig. 9(b) and (c), it is noted that for values of the similarity variable approximately below 0.025, the Nusselt number is greater for the $Da^{-1} = 5$ than for $Da^{-1} = 1.5$ (greater permeability), which could mean that when approxing $\eta \to 0$ the stretching of the boundary sheet is less relevant due to its close relation to the Darcy parameter.

The dependence of the heat transfer with the Eckert number is also worthy of study. This is illustrated in Fig. 10. This figure shows the plots for temperature and Nusselt number, which reveal that to increase the Eckert number increases the temperature and the Nusselt number, since the increase in Eckert parameter shows a significant contribution of fluid kinetic energy, which is also remarkably boosted when adding nanoparticles to the fluid with $\phi = 0.01$. As the Eckert number grows, convection becomes more relevant, leading to an increase in temperature. This is reflected in the Nusselt number: since the said increase in Eckert influences the Nusselt number by modifying the kinetic energy of the liquid, the convective heat transfer gains strong relevance over the rest heat mechanisms. For these reasons, the Eckert number is crucial in thermal management systems, especially in applications involving flows at relatively high speeds, such as aerospace or cooling systems, where temperature control is vital for optimal performance.

Fig. 10(a): Temperature graph for various values of Eckert number.

Finally, in heat transfer with nanofluids is of strong importance the volume fraction, since this makes important change of thermophysical

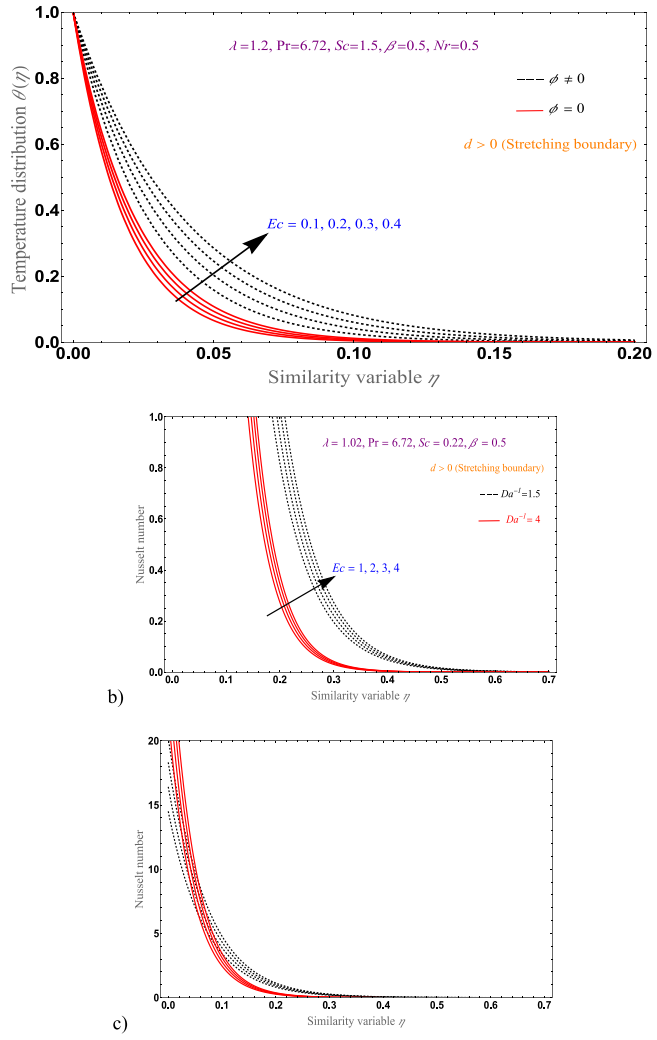

Fig. 10. Evolution with the similarity parameter when varying *Ec* for: a) temperature, and Nusselt number in zoom (b) and global view (c).

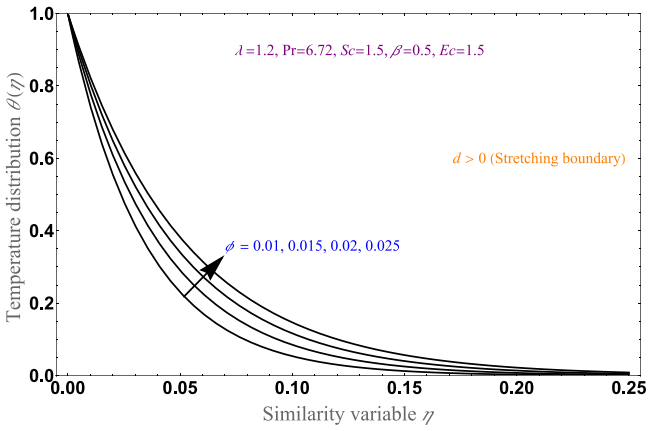

Fig. 11. Impact of the volume fraction on the temperature profile.

properties in the fluid. For this reason, Fig. 11 portrays the volume fraction plots for the temperature profile over the expanding sheet, while keeping radiation, Schmidt number, Prandtl number, and other terms constant. As expected from analyzing other works in the literature, in which the aggregation of nanoparticles increased substantially the heat transfer ability of the fluid, the temperature distribution is increased. The results in Fig. 11 show that even small volume fractions have a dramatic impact on heat transfer by increasing the temperature. Also, increasing the volume fraction parameter affects the thermal boundary layer for stretching boundary, and the thermal boundary layer thickness decays. In other words, from a physical point of view, as the volume fraction of nanoparticles increases, the thermal conductivity of the fluid grows, which is because the added nanoparticles possess higher thermal conductivity compared to the conventional fluid, enhancing the ability of the fluid to transport heat. The volume fraction is crucial in applications such as cooling systems and heat exchangers, where efficient thermal management is essential for system performance.

To conclude the present investigation, the concentration will be analysed in Fig. 12, when varying the Stefan blowing parameter with $Sc = 1$, and in Fig. 13, when varying the Schmidt number over a stretching boundary. Between these two figures, it is crystal clear that the Stefan blowing parameter plays the most important role on concentration. The concentration profiles are much more affected when increasing Λ, even with small values, than when increasing *Sc,* for either $\phi = 0$ or $\phi \neq 0$. The changes in Fig. 12 are even different than the changes in Fig. 13, showing reversed sigmoidal-like behaviours, rather than exponential-like decays. Also, as relevant aspect to point out, the ternary nanofluid shows more increase in concentration compared to the $\phi = 0$ fluid, for obvious reasons. From Fig. 13 can be also remarked that,

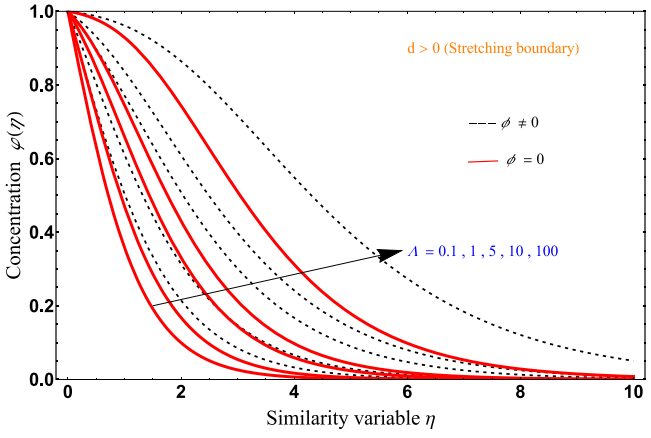

Fig. 12. Graph of concentration for variations of Stefan blowing parameter.

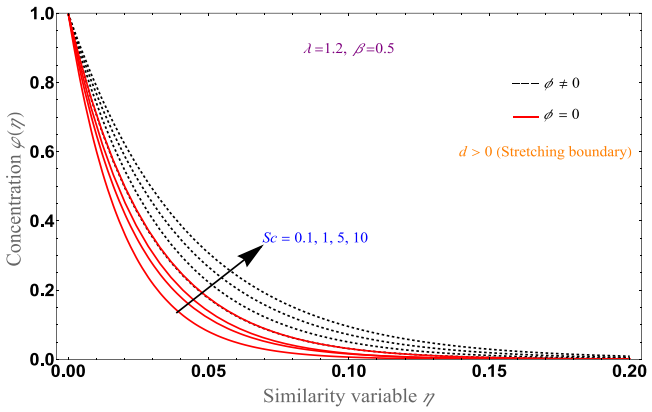

Fig. 13. Graph of concentration for variations of Schmidt number.

as the Schmidt number increases, the concentration gradient typically becomes steeper, indicating reduced mass transfer due to higher convective viscosity relative to mass diffusivity. This results in lower concentration levels in the bulk fluid, as higher *Sc* values correlate with lower mass diffusion rates. Consequently, it is evident that systems with higher Schmidt numbers exhibit slower mass transfer rates, affecting overall concentration distributions and profiles.

5. Conclusions

In this work it has been examined the effects of Stefan blowing and Schmidt number for a bi-viscous Bingham ternary nanofluid Titanium dioxide (TiO_2), Silver (Ag), (Copper (Cu) and nanoparticles in sodium alginate) over a stretching/shrinking boundary and thermal radiation. The study contains a very rich parameter exploration, which includes variations in the Stefan blowing parameter, Schmidt number, Eckert number, thermal radiation parameter or volume fraction, as well as controlling the case scenario by the Bingham parameter, inverse Darcy number and the Prandtl, with the aim of analysing relevant variables such as velocity, concentration, temperature and Nusselt profiles, as a result of using similarity transformations to the system of PDEs to transform these into nonlinear ODEs solved analytically.

The novel scientific findings derived for the first time from the current analysis are as follows:

- Despite the Bingham fluid is well-known and it is present in many industrial applications, there are no studies in literature that combine the Stefan blowing effect, Schmidt number (mass diffusion), bi-viscous Bingham ternary nanofluid (Cu, Ag and TiO2 nanoparticles mixed in sodium alginate), and radiation (via Rosseland approximation) in a porous and stretching/shrinking sheet medium. This work introduces a novel contribution by examining, for the first time, the combined influence of blowing effects resulting from substantial species transfer on fluid flow, heat, and mass transport over a stretching surface, whose corresponding energy and concentration equations are analytically solved. The analysis highlights how variations in the blowing parameter, Schmidt number affect the behaviour of velocity, temperature, and concentration fields. The derived solutions are expressed in terms of hypergeometric functions.
- The current analysis reveals that the bi-viscous Bingham ternary nanofluid outperforms the behaviour of conventional fluids. The nanofluid had greater wall concentration gradients and temperature. Also, to increase the volume fraction significantly alters the temperature distribution of the nanofluid across the stretching boundary. Additionally, the Nusselt number increases, particularly due to the rise in the Eckert number, which strongly influences convective heat transfer in the ternary nanofluid.
- To increase the thermal radiation and Eckert number increases the temperature of the fluid flow. It has been also noticed that when adding the ternary nanoparticles to the fluid with $\phi = 0.01$, the effect is strongly boosted. As the Eckert number enhances, convection becomes more relevant, leading to an increase in temperature, powered by the enhanced thermophysical capabilities of the nanoparticles.
- In accordance with previous studies, the results show that as the Stefan blowing parameter Λ increases, the value of β decreases, especially at lower Schmidt numbers, where mass diffusion becomes more dominant than momentum diffusion.
- It has been observed also that the Stefan blowing parameter provides superior control over concentration. The higher the blowing parameter, the more sensitive concentration is to the addition of nanoparticles. In other words, for higher blowing, to add even a low volume fraction of ternary nanoparticles becomes very influential to concentration.
- The Schmidt number had an important influence on the temperature distribution of the nanofluid, the Stefan blowing with respect to β/inverse Darcy number/stretching & shrinking parameter, and on concentration. The variation in the Schmidt number affected dramatically to Λ and β, thus producing evident variations and increase in the behaviour of the concentration.

With respect to the practical applications of this study, the combination of all the aforementioned effects suggests that such fluid scenarios are highly suitable for use in advanced thermal management systems. This includes e.g. applications in cooling of electronics, catalytic reactors, solar energy harvesting systems, insulation technologies, and underground heat storage units. The strong agreement with previous benchmark studies further reinforces the credibility and applicability of the results, making them a valuable reference for future experimental and industrial research.

Regarding the limitations and future scope, the current study introduces valuable insights into the influence of Stefan blowing, radiation, and non-Newtonian behaviour on transport phenomena. However, there are certain limitations, including the assumption of steady-state flow and neglecting more complex effects like variable fluid properties and higher-order non-Newtonian models. Additionally, the study focuses primarily on theoretical analysis, which may not capture the full range of real-world complexities, such as including turbulence or surface roughness. In future research would be interesting to explore the inclusion of unsteady flow conditions, more complex nanofluid models with temperature-dependent properties, and to perform experimental studies to exhibit the practical applicability of the findings. Further investigation into the impact of multiple nanofluid types and varying radiation intensities could also offer a more detailed insight of heat and mass transfer dynamics in such systems.

CRediT authorship contribution statement

Mahabaleshwar U. S.: Writing – original draft, Visualization, Supervision, Investigation, Conceptualization. **Granados-Ortiz Francisco-Javier:** Writing – review & editing, Writing – original draft, Visualization, Validation, Supervision, Investigation, Formal analysis. **Perez L. M.:** Writing – review & editing, Visualization, Conceptualization. **J. Ortega-Casanova:** Writing – review & editing, Visualization, Validation. **Sachhin S. M.:** Writing – original draft, Validation, Methodology, Investigation, Formal analysis, Conceptualization.

Declaration of Competing Interest

The corresponding author, on behalf of the authors, declares that there is no conflict of interest to his knowledge.

Acknowledgements

L.M.P. acknowledges financial support from ANID through Convocatoria Nacional Subvención a Instalación en la Academia Convocatoria Año 2021, Grant SA77210040. F.J.G.O. acknowledges the Ramón y Cajal 2021 Excellence Research Grant action from the Spanish Ministry of Science and Innovation (FSE/AGENCIA ESTATAL DE INVESTIGACIÓN).

Appendix A

Thermophysical properties of the ternary nanofluid.
The ternary nanoparticle thermophysical properties are selected according to the modelling in previous literature (see for instance [36,37,49]).

- Viscosity of the ternary nanofluid is modelled by [37,38]

$$\frac{\mu_{tnf}}{\mu_f} = \frac{1}{(1-\phi_{Ag})^{2.5}(1-\phi_{Cu})^{2.5}(1-\phi_{TiO_2})^{2.5}}, \tag{A.1}$$

- The density of the ternary nanofluid over the density of the base fluid is modelled according to the expression given in [37–39]

$$\frac{\rho_{tnf}}{\rho_f} = (1-\phi_{Ag})\left\{(1-\phi_{Cu})\left[(1-\phi_{TiO_2}) + \phi_{TiO_2}\frac{\rho_{TiO_2}}{\rho_f}\right] + \phi_{Cu}\frac{\rho_{Cu}}{\rho_f}\right\} + \phi_{Ag}\frac{\rho_{Ag}}{\rho_f}, \tag{A.2}$$

- The thermal capacitance of the ternary nanofluid is modelled according to [39]:

$$\frac{(\rho Cp)_{tnf}}{(\rho Cp)_f} = (1-\phi_{Ag})\left\{(1-\phi_{Cu})\left[(1-\phi_{TiO_2}) + \phi_{TiO_2}\frac{(\rho Cp)_{TiO_2}}{(\rho Cp)_f}\right] + \phi_{Cu}\frac{(\rho Cp)_{Cu}}{(\rho Cp)_f}\right\} + \phi_{Ag}\frac{(\rho Cp)_{Ag}}{(\rho Cp)_f}, \tag{A.3}$$

- The thermal conductivity of the nanofluid is expressed by the system of equations shown below [37],

$$\begin{aligned}
\frac{\kappa_{tnf}}{\kappa_{hnf}} &= \frac{\kappa_{Ag} + 2\kappa_{hnf} - 2\phi_{Ag}(\kappa_{hnf} - \kappa_{Ag})}{\kappa_{Ag} + 2\kappa_{hnf} + \phi_{Ag}(\kappa_{hnf} - \kappa_{Ag})},\\
\frac{\kappa_{hnf}}{\kappa_{nf}} &= \frac{\kappa_{Cu} + 2\kappa_{nf} - 2\phi_{Cu}(\kappa_{nf} - \kappa_{Cu})}{\kappa_{Cu} + 2\kappa_{nf} + \phi_{Cu}(\kappa_{nf} - \kappa_{Cu})},\\
\frac{\kappa_{nf}}{\kappa_f} &= \frac{\kappa_{TiO_2} + 2\kappa_f - 2\phi_{TiO_2}(\kappa_f - \kappa_{TiO_2})}{\kappa_{TiO_2} + 2\kappa_f + \phi_{TiO_2}(\kappa_f - \kappa_{TiO_2})},
\end{aligned} \tag{A.4}$$

Data availability

Data that support the findings of this study are available from the corresponding author upon reasonable request.

References

[1] S.M. Sachhin, U.S. Mahabaleshwar, D. Laroze, D. Drikakis, Darcy–Brinkman model for ternary dusty nanofluid flow across stretching/shrinking surface with suction/injection, Art. no. 4, Fluids 9 (4) (Apr. 2024), https://doi.org/10.3390/fluids9040094.
[2] M. Turkyilmazoglu, Buongiorno model in a nanofluid filled asymmetric channel fulfilling zero net particle flux at the walls, Int. J. Heat. Mass Transf. 126 (Nov. 2018) 974–979, https://doi.org/10.1016/j.ijheatmasstransfer.2018.05.093.
[3] A.A. Gkountas, L.Th Benos, G.N. Sofiadis, I.E. Sarris, A printed-circuit heat exchanger consideration by exploiting an Al2O3-water nanofluid: Effect of the nanoparticles interfacial layer on heat transfer, Therm. Sci. Eng. Prog. 22 (May 2021) 100818, https://doi.org/10.1016/j.tsep.2020.100818.
[4] P.G. Siddheshwar, R. Idris, C. Kanchana, D. Laroze, Rayleigh–Bénard Convection of Water-Copper and Water-Alumina Nanofluids Based on Minimal- and Higher-Mode Lorenz Models, Int. J. Bifurc. Chaos 33 (09) (Jul. 2023) 2350104, https://doi.org/10.1142/S0218127423501043.
[5] F.-J. Granados-Ortiz, L. Leon-Prieto, J. Ortega-Casanova, Computational study of the application of Al_2O_3 nanoparticles to forced convection of high-Reynolds swirling jets for engineering cooling processes, Eng. Appl. Comp. Fluid Mech. 15 (1) (Dec. 2020) 1–22, https://doi.org/10.1080/19942060.2020.1845805.
[6] M. Saleem, M.N. Tufail, Q.A. Chaudhry, Unsteady MHD Casson fluid flow with heat transfer passed over a porous rigid plate with stagnation point flow: Two-parameter Lie scaling approach, Pramana 95 (1) (Feb. 2021) 28, https://doi.org/10.1007/s12043-020-02054-0.
[7] M. Nazim Tufail, M. Saleem, Q. Ali Chaudhry, Two-parameter Lie convective Casson fluid scale study with MHD, joule heating and viscous dissipation influences, Proc. Inst. Mech. Eng. Part C. J. Mech. Eng. Sci. 235 (17) (Sep. 2021) 3199–3212, https://doi.org/10.1177/0954406220964843.
[8] M. Saleem, A. Al-Zubaidi, N. Radwan, S. Saleem, H. Adawi, Thermal effects of ternary Casson nanofluid flow over a stretching sheet: An investigation of Thomson and Troian velocity slip, Case Stud. Therm. Eng. 65 (Jan. 2025) 105561, https://doi.org/10.1016/j.csite.2024.105561.
[9] M. Saleem, M.N. Tufail, Q.A. Chaudhry, Significance of the physical quantities for the non-Newtonian fluid flow in an irregular channel with heat and mass transfer effects: Lie group analysis, Alex. Eng. J. 61 (3) (Mar. 2022) 1968–1980, https://doi.org/10.1016/j.aej.2021.07.003.
[10] H.J. Xu, et al., Review on heat conduction, heat convection, thermal radiation and phase change heat transfer of nanofluids in porous media: Fundamentals and applications, Chem. Eng. Sci. 195 (Feb. 2019) 462–483, https://doi.org/10.1016/j.ces.2018.09.045.
[11] M. Saleem, M. Hussain, M. Inc, Significance of Darcy–Forchheimer law and magnetic field on the comparison of Williamson–Casson fluid subject to an exponential stretching sheet, Int. J. Mod. Phys. B 37 (27) (Oct. 2023) 2350315, https://doi.org/10.1142/S0217979223503150.
[12] M. Saleem, Q.A. Chaudhry, A.O. Almatroud, One-parameter lie scaling study of carreau fluid flow with thermal radiation effects, Chaos Solitons Fractals 148 (Jul. 2021) 110996, https://doi.org/10.1016/j.chaos.2021.110996.
[13] Z. Iqbal and M. Saleem, "Convective heat transport features of Darcy Casson fluid flow in a vertical channel: a Lie group approach," *Waves Random Complex Media*, vol. 0, no. 0, pp. 1–14, doi: 10.1080/17455030.2022.2142694.
[14] M.N. Tufail, M. Saleem, Q.A. Chaudhry, Chemically reacting mixed convective Casson fluid flow in the presence of MHD and porous medium through group

theoretical analysis, Heat. Transf. 49 (8) (2020) 4657–4677, https://doi.org/10.1002/htj.21846.
[15] M.N. Tufail, M. Saleem, Q.A. Chaudhry, An analysis of Maxwell fluid through a shrinking sheet with thermal slip effect: a Lie group approach, Indian J. Phys. 95 (4) (Apr. 2021) 725–731, https://doi.org/10.1007/s12648-020-01745-z.
[16] U.S. Mahabaleshwar, T. Anusha, S.M. Sachhin, D. Zeidan, and S.W. Joo, "An impact of Richardson number on the inclined MHD mixed convective flow with heat and mass transfer," *Heat Transfer*, vol. n/a, no. n/a, doi: 10.1002/htj.23069.
[17] U.S. Mahabaleshwar, T. Anusha, P.H. Sakanaka, S. Bhattacharyya, Impact of Inclined Lorentz Force and Schmidt Number on Chemically Reactive Newtonian Fluid Flow on a Stretchable Surface When Stefan Blowing and Thermal Radiation are Significant, Arab. J. Sci. Eng. 46 (12) (Dec. 2021) 12427–12443, https://doi.org/10.1007/s13369-021-05976-y.
[18] F.T. Zohra, M.J. Uddin, A.I.M. Ismail, O. Anwar Bég, A. Kadir, Anisotropic slip magneto-bioconvection flow from a rotating cone to a nanofluid with Stefan blowing effects, Chin. J. Phys. 56 (1) (Feb. 2018) 432–448, https://doi.org/10.1016/j.cjph.2017.08.031.
[19] S.Z. Alamri, R. Ellahi, N. Shehzad, A. Zeeshan, Convective radiative plane Poiseuille flow of nanofluid through porous medium with slip: An application of Stefan blowing, J. Mol. Liq. 273 (Jan. 2019) 292–304, https://doi.org/10.1016/j.molliq.2018.10.038.
[20] O. Anwar Beg, F.T. Zohra, M.J. Uddin, A.I.M. Ismail, S. Sathasivam, Energy conservation of nanofluids from a biomagnetic needle in the presence of Stefan blowing: Lie symmetry and numerical simulation, Case Stud. Therm. Eng. 24 (Apr. 2021) 100861, https://doi.org/10.1016/j.csite.2021.100861.
[21] P. Rana, N. Shukla, O.A. Bég, A. Bhardwaj, Lie Group Analysis of Nanofluid Slip Flow with Stefan Blowing Effect via Modified Buongiorno's Model: Entropy Generation Analysis, Differ. Equ. Dyn. Syst. 29 (1) (Jan. 2021) 193–210, https://doi.org/10.1007/s12591-019-00456-0.
[22] M.J. Uddin, Y. Alginahi, O.A. Bég, M.N. Kabir, Numerical solutions for gyrotactic bioconvection in nanofluid-saturated porous media with Stefan blowing and multiple slip effects, Comput. Math. Appl. 72 (10) (Nov. 2016) 2562–2581, https://doi.org/10.1016/j.camwa.2016.09.018.
[23] C. Gromke, B. Blocken, Influence of avenue-trees on air quality at the urban neighborhood scale. Part I: quality assurance studies and turbulent Schmidt number analysis for RANS CFD simulations, Environ. Pollut. 196 (Jan. 2015) 214–223, https://doi.org/10.1016/j.envpol.2014.10.016.
[24] I. Calmet, J. Magnaudet, Large-eddy simulation of high-Schmidt number mass transfer in a turbulent channel flow, Phys. Fluids 9 (2) (Feb. 1997) 438–455, https://doi.org/10.1063/1.869138.
[25] C. Gualtieri, A. Angeloudis, F. Bombardelli, S. Jha, T. Stoesser, On the Values for the Turbulent Schmidt Number in Environmental Flows, Fluids 2 (Apr. 2017) 1–27, https://doi.org/10.3390/fluids2020017.
[26] U.S. Mahabaleshwar, S.M. Sachhin, L.M. Pérez, G. Lorenzini, An Effect of Mass Transpiration and Darcy–Brinkman Model on Ostwald–de Waele Ternary Nanofluid, J. Engin. Thermophys. 33 (3) (Sep. 2024) 547–565, https://doi.org/10.1134/S181023282403010X.
[27] T. Fang, W. Jing, Flow, heat, and species transfer over a stretching plate considering coupled Stefan blowing effects from species transfer, Commun. Nonlinear Sci. Numer. Simul. 19 (9) (Sep. 2014) 3086–3097, https://doi.org/10.1016/j.cnsns.2014.02.009.
[28] S.M. Sachhin, U.S. Mahabaleshwar, S.N.R. Nayakar, H.S.R. Patil, and B. Souayeh, "Darcy–Brinkman model for Boussinesq–Stokes suspension tetra dusty nanofluid flow over stretching/shrinking sheet with suction/injection," *Numerical Heat Transfer, Part A: Applications*, vol. 0, no. 0, pp. 1–23, doi: 10.1080/10407782.2024.2359047.
[29] F. Asmat, W.A. Khan, I. Usman, Khan, T. Muhammad, A scientific report on Stokes' second problem for a transient nanofluid model with a heated boundary in the presence of a magnetic field, J. Magn. Magn. Mater. 586 (Nov. 2023) 171171, https://doi.org/10.1016/j.jmmm.2023.171171.
[30] A. Razaq, S.A. Khan, A. Alsaedi, T. Hayat, Entropy induced flow model for solar radiation through nanomaterials with cubic autocatalysis reaction, J. Magn. Magn. Mater. 586 (Nov. 2023) 171172, https://doi.org/10.1016/j.jmmm.2023.171172.
[31] A. Lakouader, et al., Impact of polymeric precursor and auto-combustion on the structural, microstructural, magnetic, and magnetocaloric properties of La0.8Sr0.2MnO3, J. Magn. Magn. Mater. 586 (Nov. 2023) 171225, https://doi.org/10.1016/j.jmmm.2023.171225.
[32] L. Regeciová, P. Farkašovský, Magnetization processes and magnetocaloric effect of the Ising model on the octahedral lattice, J. Magn. Magn. Mater. 586 (Nov. 2023) 171153, https://doi.org/10.1016/j.jmmm.2023.171153.
[33] S.E. Ahmed, et al., Magnetohydrodynamic convection-entropy generation of a non-Newtonian nanofluid in a 3D chamber filled with a porous medium, J. Magn. Magn. Mater. 586 (Nov. 2023) 171175, https://doi.org/10.1016/j.jmmm.2023.171175.
[34] J. Queiros Campos, et al., Physical aspects of magnetic nanoparticle manipulation in environmental and biomedical applications, J. Magn. Magn. Mater. 586 (Nov. 2023) 171162, https://doi.org/10.1016/j.jmmm.2023.171162.
[35] K. Hiemenz, "Die Grenzschicht an einem in den gleichförmigen Flüssigkeitsstrom eingetauchten geraden Kreiszylinder," Accessed: Aug. 28, 2024. [Online]. Available: ⟨https://www.semanticscholar.org/paper/Die-Grenzschicht-an-einem-in-den-gleichf%C3%B6rmigen-Hiemenz/d864aec54cab42216097b9b4d8f7519d377b616e⟩.
[36] Th.V. Kármán, Über laminare und turbulente Reibung, ZAMM J. Appl. Math. Mech. Z. F. üR. Angew. Math. Mech. 1 (4) (Jan. 1921) 233–252, https://doi.org/10.1002/zamm.19210010401.
[37] N. Sarwar, S. Jahangir, M.I. Asjad, S.M. Eldin, Application of ternary nanoparticles in the heat transfer of an MHD non-newtonian fluid flow, Micromachines 13 (12) (Dec. 2022) 2149, https://doi.org/10.3390/mi13122149.
[38] S.M. Sachhin, U.S. Mahabaleshwar, N. Swaminathan, D. Laroze, L. Pedraja-Rejas, An effect of waste discharge concentration and electromagnetic field on chemically reactive Bingham fluid flow with the analysis entropy generation and mass transfer, Hybrid. Adv. 8 (Mar. 2025) 100344, https://doi.org/10.1016/j.hybadv.2024.100344.
[39] K. Kalidasan, R. Velkennedy, P. Rajesh Kanna, Laminar natural convection of copper - titania/water hybrid nanofluid in an open ended C - shaped enclosure with an isothermal block, J. Mol. Liq. 246 (Nov. 2017) 251–258, https://doi.org/10.1016/j.molliq.2017.09.071.
[40] L.J. Crane, Flow past a stretching plate, Z. F. üR. Angew. Math. Phys. ZAMP 21 (4) (Jul. 1970) 645–647, https://doi.org/10.1007/BF01587695.
[41] K. Pavlov, "Magnetohydrodynamic flow of an incompressible viscous fluid due to deformation of a plane surface," 1974. Accessed: Aug. 28, 2024. [Online]. Available: ⟨https://www.semanticscholar.org/paper/Magnetohydrodynamic-flow-of-an-incompressible-fluid-Pavlov/7f153b13f39ee3bb8fb5d18eb55a36718d7acf1c⟩.
[42] U. Khan, et al., Exact solutions for MHD axisymmetric hybrid nanofluid flow and heat transfer over a permeable non-linear radially shrinking/stretching surface with mutual impacts of thermal radiation, Eur. Phys. J. Spec. Top. 231 (6) (Jun. 2022) 1195–1204, https://doi.org/10.1140/epjs/s11734-022-00529-2.
[43] M. Turkyilmazoglu, A note on micropolar fluid flow and heat transfer over a porous shrinking sheet, Int. J. Heat. Mass Transf. 72 (May 2014) 388–391, https://doi.org/10.1016/j.ijheatmasstransfer.2014.01.039.
[44] W. Khan, E.H. Aly, Multiple exact solutions for micropolar slip flow and heat transfer of a bidirectional moving plate, SSRN Electron. J. (2022), https://doi.org/10.2139/ssrn.4142199.
[45] A. Dawar, Z. Shah, W. Khan, M. Idrees, S. Islam, Unsteady squeezing flow of magnetohydrodynamic carbon nanotube nanofluid in rotating channels with entropy generation and viscous dissipation, Adv. Mech. Eng. 11 (1) (Jan. 2019) 1687814018823100, https://doi.org/10.1177/1687814018823100.
[46] M. Sheikholeslami, Z. Shah, A. Shafee, P. Kumam, H. Babazadeh, Lorentz force impact on hybrid nanofluid within a porous tank including entropy generation, Int. Commun. Heat. Mass Transf. 116 (Jul. 2020) 104635, https://doi.org/10.1016/j.icheatmasstransfer.2020.104635.
[47] R. Naz, S. Tariq, M. Sohail, Z. Shah, Investigation of entropy generation in stratified MHD Carreau nanofluid with gyrotactic microorganisms under Von Neumann similarity transformations, Eur. Phys. J. 135 (2) (Feb. 2020) 178, https://doi.org/10.1140/epjp/s13360-019-00069-0.
[48] S.O. Alharbi, et al., Entropy generation in MHD eyring–powell fluid flow over an unsteady oscillatory porous stretching surface under the impact of thermal radiation and heat source/sink, Art. no. 12, Appl. Sci. 8 (12) (Dec. 2018), https://doi.org/10.3390/app8122588.
[49] M. Jawad, et al., Impact of Nonlinear Thermal Radiation and the Viscous Dissipation Effect on the Unsteady Three-Dimensional Rotating Flow of Single-Wall Carbon Nanotubes with Aqueous Suspensions, Art. no. 2, Symmetry 11 (2) (Feb. 2019), https://doi.org/10.3390/sym11020207.
[50] T. Salahuddin, M. Awais, Thermal and solutal transport by Cattaneo-Christov model for the magnetohydrodynamic Williamson fluid with joule heating and heat source/sink, Heliyon 10 (7) (Apr. 2024) e29228, https://doi.org/10.1016/j.heliyon.2024.e29228.
[51] T. Salahuddin, M. Awais, Numerical computation of joule heating and chemical reaction for the radiated Casson fluid on the slender parabolic surface, ZAMM J. Appl. Math. Mech. Z. F. üR. Angew. Math. Mech. 104 (4) (2024) e202300647, https://doi.org/10.1002/zamm.202300647.
[52] M. Awais, T. Salahuddin, Radiative magnetodydrodynamic cross fluid thermophysical model passing on parabola surface with activation energy, Ain Shams Eng. J. 15 (1) (Jan. 2024) 102282, https://doi.org/10.1016/j.asej.2023.102282.
[53] M. Awais, T. Salahuddin, Natural convection with variable fluid properties of couple stress fluid with Cattaneo-Christov model and enthalpy process, Heliyon 9 (8) (Aug. 2023) e18546, https://doi.org/10.1016/j.heliyon.2023.e18546.
[54] T. Salahuddin, M. Awais, Natural convective and Cattaneo–Christov model for couple stress nanofluid at the middle of the squeezed channel with sensor surface, Int. J. Mod. Phys. B 38 (32) (Dec. 2024) 2450443, https://doi.org/10.1142/S0217979224504435.
[55] T. Salahuddin, M. Awais, Implementing the predictor-corrector approach to examine the thermo-solutal convection for buongiorno eyring-powell nanofluid model with squeezed microcantilivier surface, Alex. Eng. J. 108 (Dec. 2024) 40–49, https://doi.org/10.1016/j.aej.2024.07.033.
[56] T. Salahuddin, M. Awais, S. Muhammad, Featuring the aspects with temperature dependent viscosity of inclined MHD Williamson fluid along with heat source/sink, soret and dufour effects: a predictor-corrector approach, Int. Commun. Heat. Mass Transf. 159 (Dec. 2024) 108178, https://doi.org/10.1016/j.icheatmasstransfer.2024.108178.
[57] M. Awais, T. Salahuddin, M.O. Sidi, A.A. Agha, H.A. Garalleh, Insight into thermal dynamic of stagnated flow of MHD Jeffery fluid when the joule heating, viscous dissipation and Soret effect are present: a multistep Milne's approach, Case Stud. Therm. Eng. 64 (Dec. 2024) 105506, https://doi.org/10.1016/j.csite.2024.105506.
[58] Md.J. Uddin, O.A. Bég, A.I. Ismail, Radiative Convective Nanofluid Flow Past a Stretching/Shrinking Sheet with Slip Effects, J. Thermophys. Heat. Transf. 29 (3) (Jul. 2015) 513–523, https://doi.org/10.2514/1.T4372.

[59] O.A. Bég, D. Kumar, M.J. Uddin, M.A. Alim, T.A. Bég, Simulation of magneto-nano-bioconvective coating flow with blowing and multiple slip effects, Proc. Inst. Mech. Eng. Part N. J. Nanomater. Nanoeng. Nanosyst. (Jul. 2024) 23977914241259815, https://doi.org/10.1177/23977914241259815.

[60] W.A. Khan, M.J. Uddin, Nano-bioconvective anisotropic slip flow in anisotropic porous medium with Coriolis force effects, Heat. Transf. 53 (2) (2024) 558–583, https://doi.org/10.1002/htj.22963.

[61] M.J. Uddin, N.H.M. Yusoff, O. Anwar Bég, A.I. Ismail, Lie group analysis and numerical solutions for non-Newtonian nanofluid flow in a porous medium with internal heat generation, Phys. Scr. 87 (2) (Jan. 2013) 025401, https://doi.org/10.1088/0031-8949/87/02/025401.

[62] M.J. Uddin, W.A. Khan, A.I. Md. Ismail, O. Anwar Bég, Computational study of three-dimensional stagnation point nanofluid bioconvection flow on a moving surface with anisotropic slip and thermal jump effect (no), J. Heat. Transf. 138 (Jun. 2016) 104502, https://doi.org/10.1115/1.4033581.

[63] W.A. Khan, I. Pop, Boundary-layer flow of a nanofluid past a stretching sheet, Int. J. Heat. Mass Transf. 53 (11) (May 2010) 2477–2483, https://doi.org/10.1016/j.ijheatmasstransfer.2010.01.032.

[64] C.Y. Wang, Free convection on a vertical stretching surface, ZAMM J. Appl. Math. Mech. Z. F. üR. Angew. Math. Mech. 69 (11) (1989) 418–420, https://doi.org/10.1002/zamm.19890691115.